ERDC/ITL TR-08-2

Information Technology Laboratory

US Army Corps of Engineers®
Engineer Research and Development Center

Limiting Impact Force Due to Yielding and Buckling of the Plates and Internal Structural Frame at the Impact Corner of the Barge during Its Glancing Blow Impact with a Lock Approach Wall

Robert M. Ebeling and Terry W. Warren

November 2008

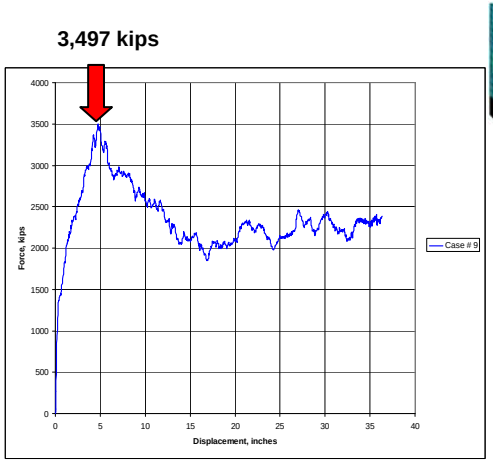

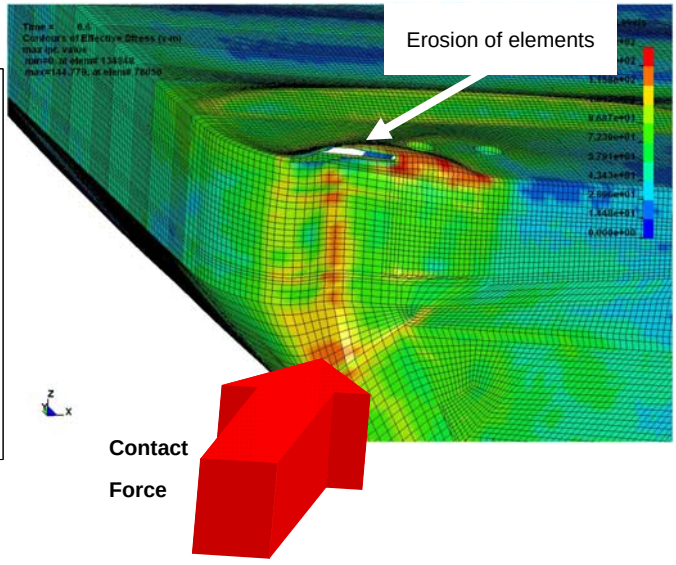

COVER: (Top) The elliptical corner region of a new jumbo open-hopper barge that will be the object of glancing blow impacts. (Bottom) Computed results from a barge corner glancing blow LS-DYNA nonlinear finite element analysis. These results are for an approach angle of 10° and a 3-ft/sec approach velocity (0.9 ft/sec velocity normal to the approach wall). (Bottom left) The results shown are the Normal Force versus Displacement curve (from zero to 36 in. of permanent deformation of the elliptical corner) with the maximum normal force highlighted. (Bottom right) The von Mises stress distribution at the time of maximum normal force. Note the computation of a crack at the elliptical corner plates, designated in this figure as “erosion of elements.”

ERDC/ITL TR-08-2
November 2008

Limiting Impact Force Due to Yielding and Buckling of the Plates and Internal Structural Frame at the Impact Corner of the Barge during Its Glancing Blow Impact with a Lock Approach Wall

Robert M. Ebeling and Terry W. Warren

Information Technology Laboratory
U.S. Army Engineer Research and Development Center
3909 Halls Ferry Road
Vicksburg, MS 39180-6199

Final report

Prepared for Headquarters, U.S. Army Corps of Engineers
Washington, DC 20314-1000

Under Work Unit 0HB385

Abstract: In 2003, the U.S. Army Corps of Engineers issued ERDC/ITL TR-03-3, which interpreted eight of the 44 full-scale, low-velocity, controlled-impact barge train experiments conducted at the decommissioned Gallipolis Lock at Robert C. Byrd Lock and Dam. An easy-to-use "empirical correlation" was derived, reporting the maximum impact force (normal to the wall) as a function of the linear momentum normal to the wall (immediately before impact). This empirical correlation was cited in ETL 1110-2-563 (April 2004) for impacts with stiff-to-rigid walls that do not involve damage to either the corner barge or the wall; a limiting impact force of 800 kips (capping the empirical correlation) was cited. In this technical report, we provide a basis for revising the "capping force" cited in ETL 1110-2-563, based on the computation of the "crushing" force imparted during a glancing blow of the impact corner at the bow with a lock approach wall.

A second limiting force due to the limit state of lashing forces during a glancing blow impact is addressed in the USACE technical report ERDC/ITL TR-05-1. The lower of the two limiting forces—due to the crushing of the barge impact corner or to the failure of the lashings—"caps" the empirical correlation.

Contents

Figures and Tables

Figures

Tables

Preface

Funding to initiate research and software development was provided by Headquarters, U.S. Army Corps of Engineers (HQUSACE), as part of the Infrastructure Technology Research Program. Funding to conclude this research task, including software development, was provided by the Navigation Systems Research Program. The research was performed under Work Unit 0HB385, entitled "Vessel/Barge Impact," for which Dr. Robert M. Ebeling, Engineering Informatics Systems Division (EISD), Information Technology Laboratory (ITL), Engineer Research and Development Center (ERDC), was the principal investigator. The HQUSACE technical monitor was Anjana Chudgar, CECW-CE.

James Clausner, Coastal and Hydraulics Laboratory (CHL), ERDC, was the Navigation Systems Research Program manager and Dr. John Hite was the inland focus area leader. Dr. Michael Sharp was acting technical director for Navigation. Angela Premo was the Navigation business line leader, HQUSACE.

The authors thank Dr. Richard Weed, ERDC computational structural mechanics on-site for the Department of Defense High-Performance Computing Modernization Program (HPCMP) User Productivity Enhancement and Technology Transfer (PET), for his support during the development of the finite element model of the barge and his advice on running LS-DYNA. The authors also thank Robert Alter, ERDC High-Performance Computing (HPC) Major Shared Resource Center (MSRC) lead (LM), for his assistance with setting up script files and batch jobs on the high-performance computers at ERDC MSRC.

This report was prepared by Dr. Robert M. Ebeling (ERDC, ITL) and Terry W. Warren (ITL). Dr. Ebeling was author of the scope of work for this research. The report was prepared by Dr. Ebeling under the supervision of Dr. Robert M. Wallace, Chief, EISD, ITL and Dr. Reed Mosher, Director, ITL.

COL Gary E. Johnston was Commander and Executive Director of ERDC. Dr. James R. Houston was Director.

Unit Conversion Factors

Multiply	By	To Obtain
feet	0.3048	meters
pounds (force)	4.448222	newtons
pounds (force) per inch	175.1268	newtons per meter
tons (force)	8,896.443	newtons

1 Introduction

1.1 Background: barge train maximum impact forces

Locks are a necessary structural feature found at every dam within the U.S. inland waterways navigation system. This network of rivers is an essential component of the nation's transportation infrastructure system, a system key to national commerce. Locks allow for groups of barges, lashed together to form barge trains, to negotiate the changes in river elevation at the dams. One of the most frequent loads applied to the locks of the U.S. inland waterway system is the impact made by a barge train on the approach walls as the barge train aligns itself to transit the lock. Consequently, this load case represents one of the primary design loads considered for lock approach walls.

This research report discusses the results of a series of nonlinear finite element analyses computing the limiting impact force due to yielding and buckling of the deck and skin plates and the internal structural frame within the "impact corner" of the bow of a jumbo open-hopper barge during a glancing blow impact with a lock approach wall. The "structural concept" can be explained as follows. Because of the elasto-plastic and limiting strain material characteristics of steel—combined with the structural layout of the deck and hull plate, the internal structural plates, and the angle steel of the internal trusses—the multi-degree-of-freedom structure of the barge bow provides a limiting force resistance during an impact event. When placed in a severe-impact environment, in which the impact corner of the bow begins to "crush," the barge bow will act like a structural "fuse-plug" to provide for a limiting impact force applied to the approach wall by the barge train. Thus, there is an upper-bound force that approach walls will be subjected to during a glancing blow impact event. This report summarizes the research effort investigating the magnitude of this limiting force. The barge used in this study is a rake section, jumbo open-hopper barge 200-ft long, 35-ft wide, and 13-ft high at the hopper section region.

1.1.1 Empirical correlation

Lock approach walls are designed for usual, unusual, and extreme loads. In the past, the primary focus of engineers performing impact computations has been on the lock approaches where the worst-case events and damage to

the barge train and/or wall are likely to occur (e.g., extreme loads where vessel control is lost). The U.S. Army Corps of Engineer's (USACE) initial guidance, engineer technical letter ETL 1110-2-338, for computing glancing-blow maximum impact forces for barge trains impacting approach walls was rescinded in 2001. The impact force computations in ETL 1110-2-338 were based on crushing of the impact corner of the barge, a response that is usually associated with an extreme load case, and not the no-damage usual load case, nor the minor damage unusual load case. In April 2004, ETL 1110-2-563 "Barge Impact Analysis for Rigid Walls" was issued by Headquarters, USACE. The impact force computations are based on the "empirical correlation" developed by Arroyo et al. (2003), shown in Figure 1.1. Details regarding its development are summarized in Appendix A.

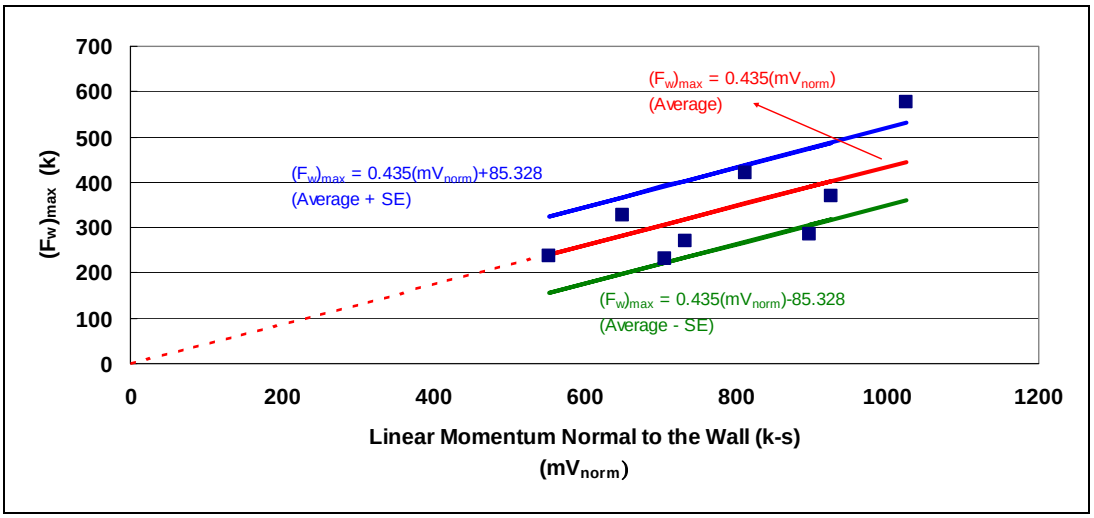

Figure 1.1. Empirical correlation using the linear momentum normal to the wall concept; from Figure 6.3 in Arroyo et al. (2003).

This figure reflects advances in the computations of usual and some unusual impact design loads during which no damage occurs to the wall and the barges, and no failure occurs in the lashings that bind the barges. The reduction of the Patev et al. (2003) load data measured during full-scale, low-velocity, controlled-impact barge experiments using a 3-by-5 (three wide and five long) 15-barge train impacting a wall at a decommissioned USACE lock is discussed in Arroyo et al. (2003), along with the resulting empirical correlation. Figure 1.1 idealizes the interrelationship between maximum impact force imparted to the wall and the linear momentum (immediately before impact) of the barge train normal to the wall. Linear momentum conveniently represents two key demand variables: the mass of the barge train and its velocity normal to the wall.

The empirical correlation in Figure 1.1 is shown to be unbounded. In actuality, it is bounded by a limiting force that functions as an asymptote to the empirical correlation, as idealized in Figure 1.2.

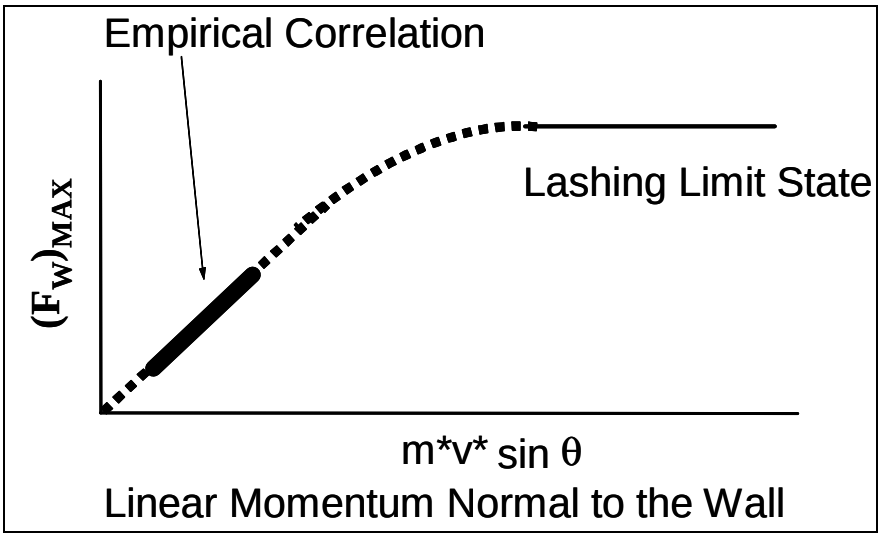

Figure 1.2. Asymptote to the empirical correlation.

This limiting impact force in Figure 1.2 results from either:

- the failure of the lashings that bind the barges of the barge train together, or
- the plastic yielding of the structural members (i.e., yielding and buckling of the deck and skin plates and the internal structural frame) in the corner of the barge that impacts the approach wall.

Whichever limiting impact force value is less becomes the limiting force to the empirical correlation in Figure 1.1. A limiting impact force of 800 kips, based on engineering judgment, was cited in the 2004 initial version of ETL 1110-2-563.

Since 2004, there has been additional research into the limiting impact force due to the failure of the lashings for various sizes of barge trains. Arroyo and Ebeling (2004) developed and fully described the theory for two probable idealized lashing failure mechanisms during a glancing blow impact with an approach wall. They are described as the transverse and corner failure mechanisms. This formulation was implemented by Arroyo and Ebeling in the PC software program Limit_LASHING. Arroyo and Ebeling (2005) present a full assessment and a parametric study of these failure mechanisms. The parametric study is used to quantify the magnitude

of the maximum impact force as a function of a range of values of each of the primary variables within the barge train system. This parametric study was based on a numerical model for computing barge impact forces based on the ultimate strength of the lashings between barges, computed using the personal computer software program Limit_LASHING. This numerical study resulted in the computation of limiting impact forces below and above the 800-kips limiting force cited in the 2004 version of ETL 1110-2-563. The value for the limiting force due to lashing failures was dependent upon the size of the barge train, the size of the wire rope (i.e., lashing), the orientation of the lashing layout connecting the barges, the number of wraps around the bits, and whether the rope was new or used. The results of the numerous parametric analyses are presented in graphical form in Arroyo and Ebeling (2005).

This research report extends the limiting impact force due to lashing failures to a discussion of results for a series of LS-DYNA nonlinear finite element analyses, computing the limiting impact force due to yielding and buckling of the deck and skin plates and the internal structural frame in the front corner (e.g., Figure 1.3) of a jumbo open-hopper barge that impacts the wall. With the results of the Arroyo and Ebeling (2005) parametric study and those contained in this report, the limiting impact force for the empirical correlation may now be established for a barge train of a given size.

1.1.2 Yielding and plate buckling analyses

In the LS-DYNA nonlinear finite element analyses discussed in this report, the impact corner of the barge and the approach wall (modeled as a non-penetrating “rigid” structure) are brought into contact with one another at a constant velocity in the numerical simulation of the “crushing” of the impact corner of the barge. “Crushing” of the elliptical impact corner continues until 36 in. of penetration of the approach wall into the barge impact corner is achieved. Figure 1.4 (top) shows an overhead view of the barge impact corner at initial contact with the wall in the numerical analysis using LS-DYNA; Figure 1.4 (bottom) shows an overhead view of the barge impact corner after 36 in. of penetration for one of the numerical evaluations. Figure 1.5 shows the corresponding resultant contact force normal to the “rigid” wall, as computed by LS-DYNA during the course of this numerical analysis. The key observation is that the contact force

Figure 1.3. View of the impact corner of the jumbo open-hopper barge used in this numerical study.

between the "rigid" nonpenetrating approach wall and the elliptical impact corner increases in magnitude with wall deformation into the barge up to a peak force value: the limiting contact force. This limiting contact force value becomes the asymptote to the empirical correlation in Figure 1.1, as idealized in Figure 1.2.

Figure 1.5 is an example of typical resultant contact force normal to the "rigid" (approach) wall versus permanent deformation computed at the impact corner of the barge in the LS-DYNA nonlinear numerical analyses. In this figure, the normal force ranges in value from 0 kips to a maximum force of 3,497 kips at 4.8 in. of permanent normal deformation at the impact corner. All LS-DYNA analyses were continued out to 36 in. of permanent deformation of the rigid wall into the impact corner of the barge.

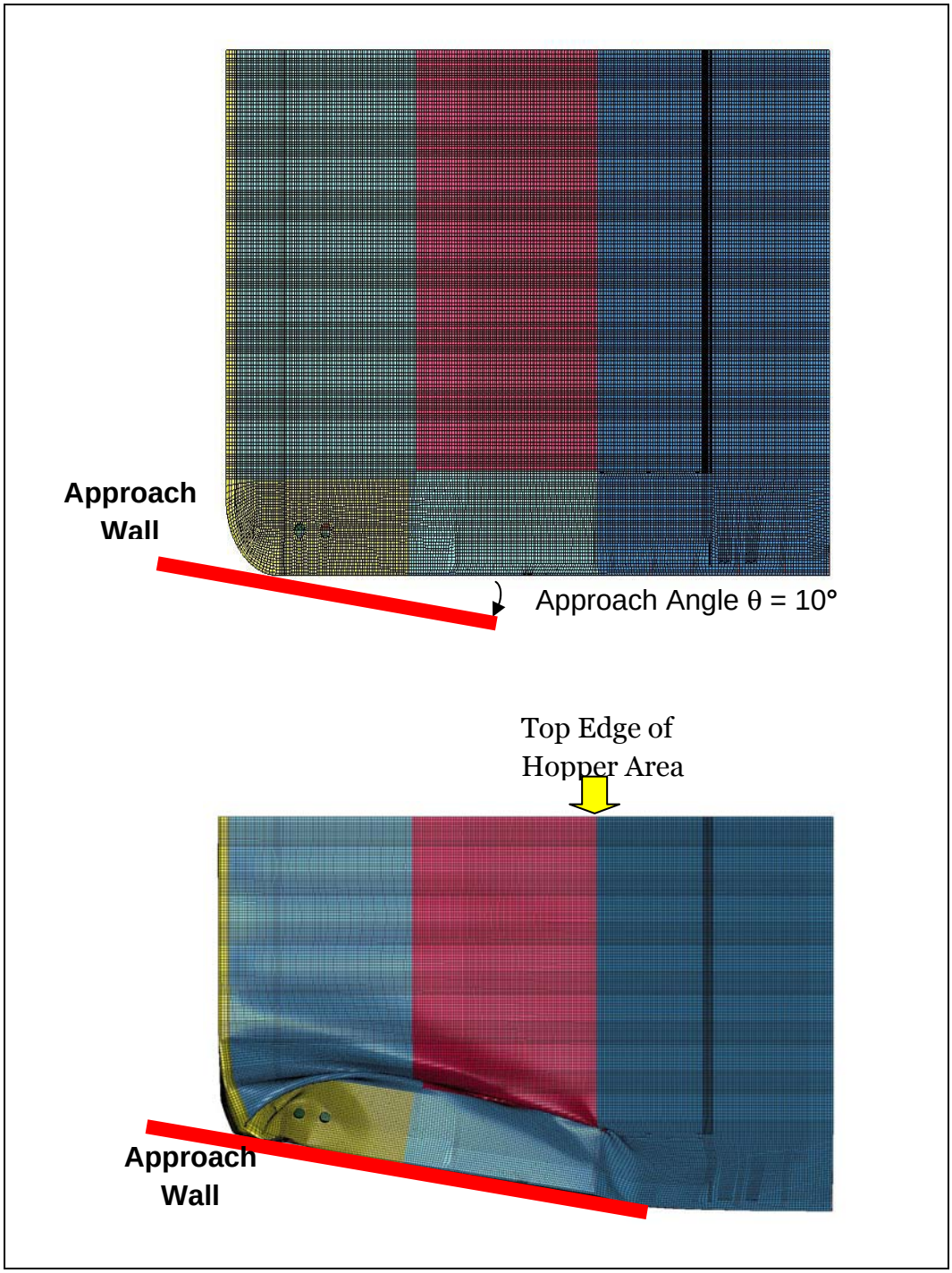

Figure 1.4. Overhead views of the barge impact corner at initial contact with the wall (top) and after 36 in. of penetration (bottom).

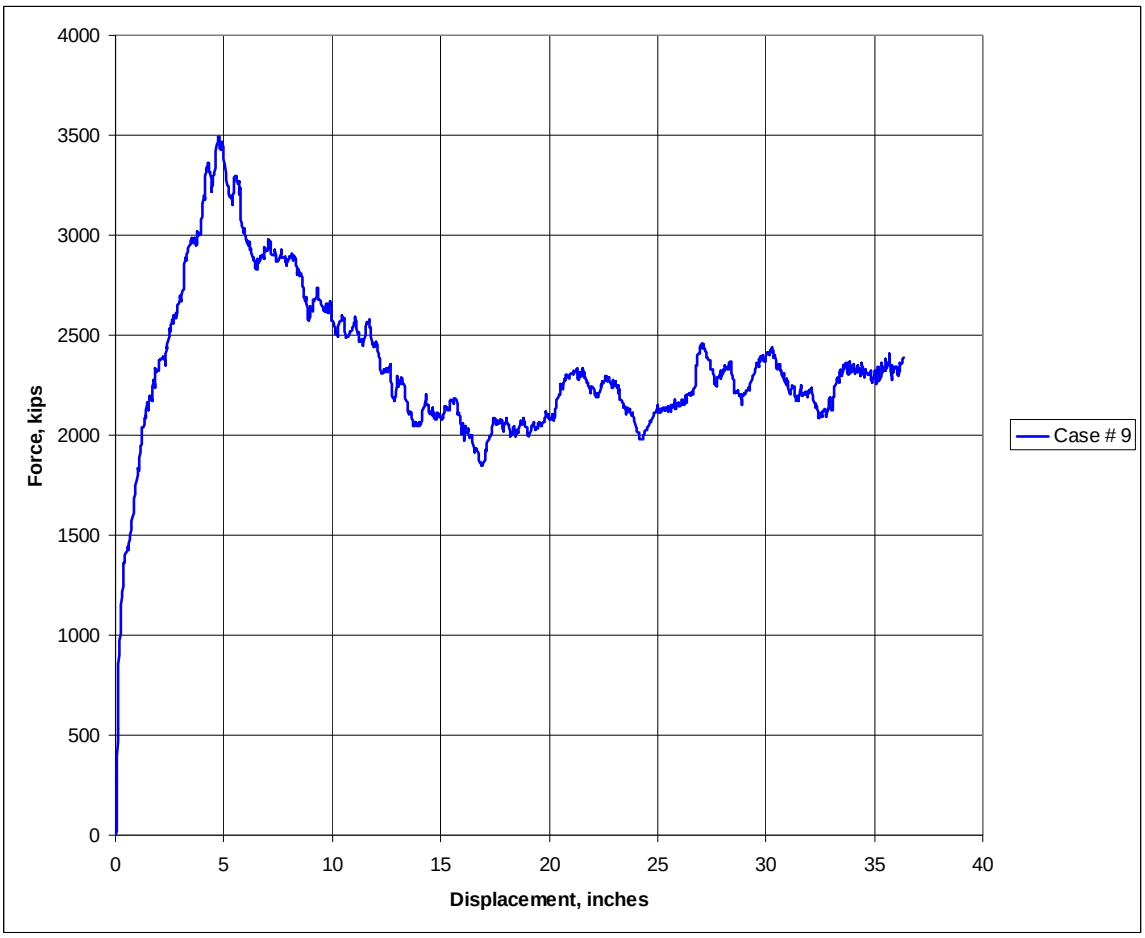

Figure 1.5. Force versus displacement of the impact corner for Case No. 9. Unusual loading condition with an approach angle of 10°.

1.2 Nonlinear structural dynamic analyses using LS-DYNA

LS-DYNA is a general purpose transient finite element program that is used for analyzing complex structural dynamics problems, such as the crushing of the impact corner of the bow of a barge during a glancing blow impact with an approach wall. It uses a central difference scheme to solve the equation of motion in time. Key features used in the analyses discussed in this report are nonlinear dynamics, use of a nonlinear elastic-plastic constitutive model for all (A-36) steel plates and angles comprising the barge, and use of contact surface formulation for a flexible-body-to-rigid-body contact. Lagrangian shell elements are used to model the barge components.

1.3 Report contents

Chapter 2 discusses the finite element mesh for the bow of the jumbo open-hopper barge assembled using TrueGRID (Rainsberger 2006) and modeled in the nonlinear LS-DYNA analyses as well as the assigned material properties. Material properties corresponding to A-36 steel, obtained from tests conducted on plate steel from a barge, are assigned in these numerical analyses.

Chapter 3 reports on the results of the 24 LS-DYNA nonlinear finite element analyses. The approach angle of the barge with the approach wall, as well as the approach velocity, is varied among the analyses.

Summary and conclusions are contained in Chapter 4.

Appendix A discusses the background for the full-scale, low-velocity controlled-impact barge experiments and the development of the empirical correlation.

Appendix B discusses the results of an evaluation of influence of the number of processors and the accuracy of computed results for the nonlinear analyses using fully integrated shell elements and reduced integration elements with hourglass control.

2 Finite Element Mesh and Material Properties

2.1 Introduction

This chapter discusses the development of the finite element mesh and the material properties assigned to the structural steel comprising the barge. The object of the nonlinear finite element analysis (using LS-DYNA) is to compute the limiting impact force due to the yielding and buckling of the plates and internal structural framing at the impact corner of the barge during its glancing blow impact with a lock approach wall; therefore, only the bow region of the jumbo open-hopper barge needs to be modeled in the numerical analysis (Figure 2.1, raked section). Additionally, because the nonlinear deformations are concentrated in the front half of the bow region closest to the impact corner, only half the bow is modeled in the analysis.

Figure 2.1. Elliptical impact corner and bow of a raked section, jumbo open-hopper bow.

This half-bow section is 17.5-ft wide and 27.7-ft long. The bow is 15.5-ft high; at the intersection of the inclined open-hopper face with the flat hopper base, the barge is 13-ft high.

2.2 Finite element mesh

The finite element software TrueGRID is used to construct the finite element mesh of the bow of the jumbo open-hopper barge. Fully integrated LS-DYNA shell elements (*SECTION_SHELL; ELFORM 16) are used in a detailed model (Figure 2.1) of the jumbo open-hopper barge bow structural steel deck, hull, and internal structural plates, as well as the internal angle steel comprising the internal structural trusses.[1] The mesh consists of 179,238 nodes and 177,241 elements. The resulting mesh of the front half of the bow of the barge is shown in Figures 2.2–2.5. Also identified in these figures (by color designation) are the thicknesses of the structural deck, hull, and hopper plates of the bow of the jumbo open-hopper barge. The headlog and elliptical impact corner sections of the bow are shown in yellow in Figures 2.3 and 2.5. The rounded hull plate connecting the front and side hull plates (in blue) is shown in brown in Figures 2.2 and 2.3. With the mesh terminating along the center line of the bow of the barge, Figure 2.4 allows for a view of the internal truss system within the bow of the barge as well as the deck and hull plates. There are seven internal trusses (six "standard" longitudinal and one outboard longitudinal truss) contained within this half-bow structural section model. The trusses are made out of A-36 steel angles. Figure 2.6(a) provides an internal view of the actual structural trusses and elliptical (impact) corner at the bow of the barge whereas Figure 2.6(b) shows the corresponding view of the structural model. Figure 2.7 (left) shows the view of the elliptical corner during its assemblage and without the deck plate, whereas Figure 2.7 (right) shows the corresponding mesh. Figure 2.8 shows the internal structural members with the deck and hull plates removed.

[1] LS-DYNA reduced integrated shell elements (*SECTION_SHELL; ELFORM = 2; NUMBER OF INTEGRATION POINTS = 3) with hourglass control (*HOURGLASS; Hourglass Control Type = 4, Flanagan-Belytschko stiffness form) were tried to save on execution time. Reduced integration resulted in execution times nearly one-third that for the fully integrated elements. However, the results obtained varied significantly if the number of processors used to run a problem was varied. Therefore, the fully integrated shell element model, used as the result obtained from runs with varying numbers of processors, was observed to be more consistent.

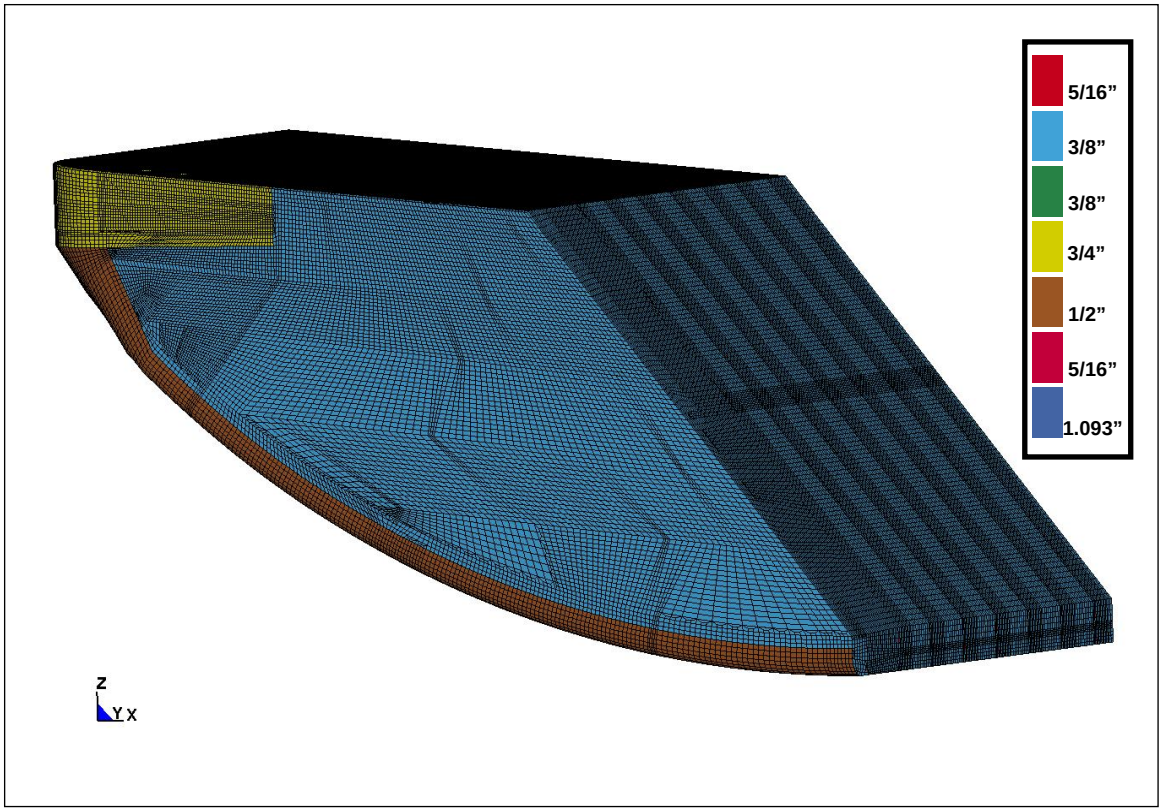

Figure 2.2. Mesh of bow—side view of the hull and hopper plates.

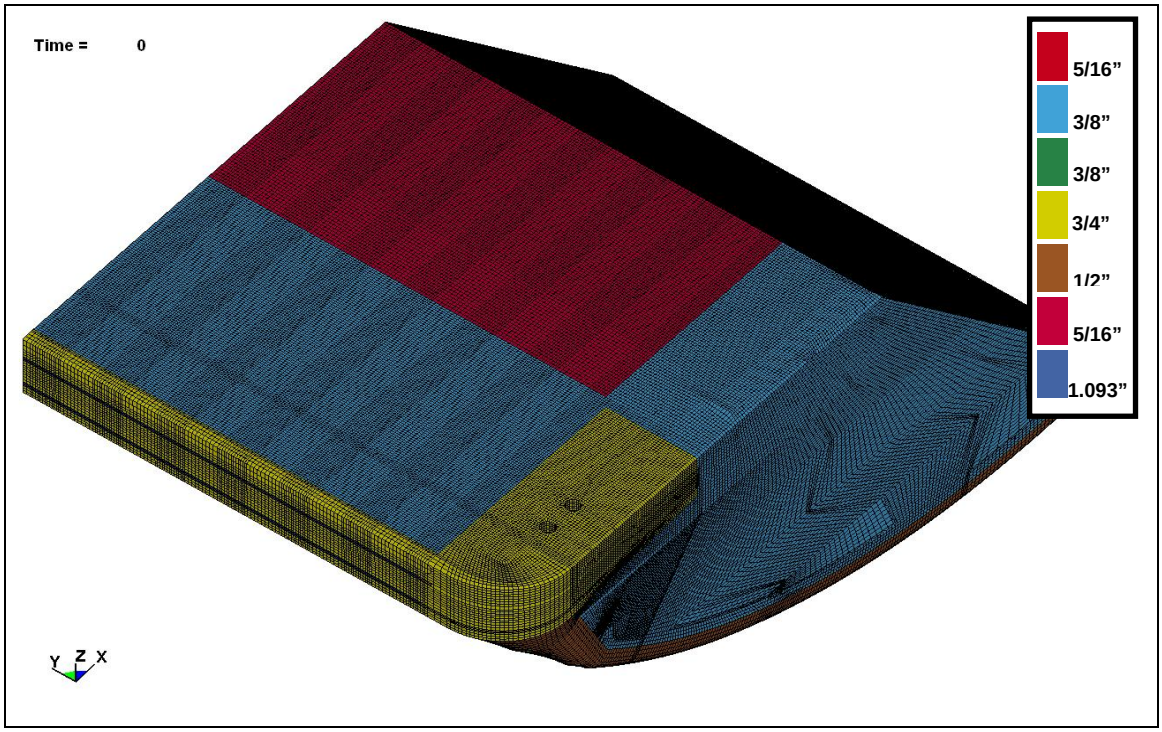

Figure 2.3. Front elliptical corner view of the deck plates, headlog, and elliptical corner of the bow.

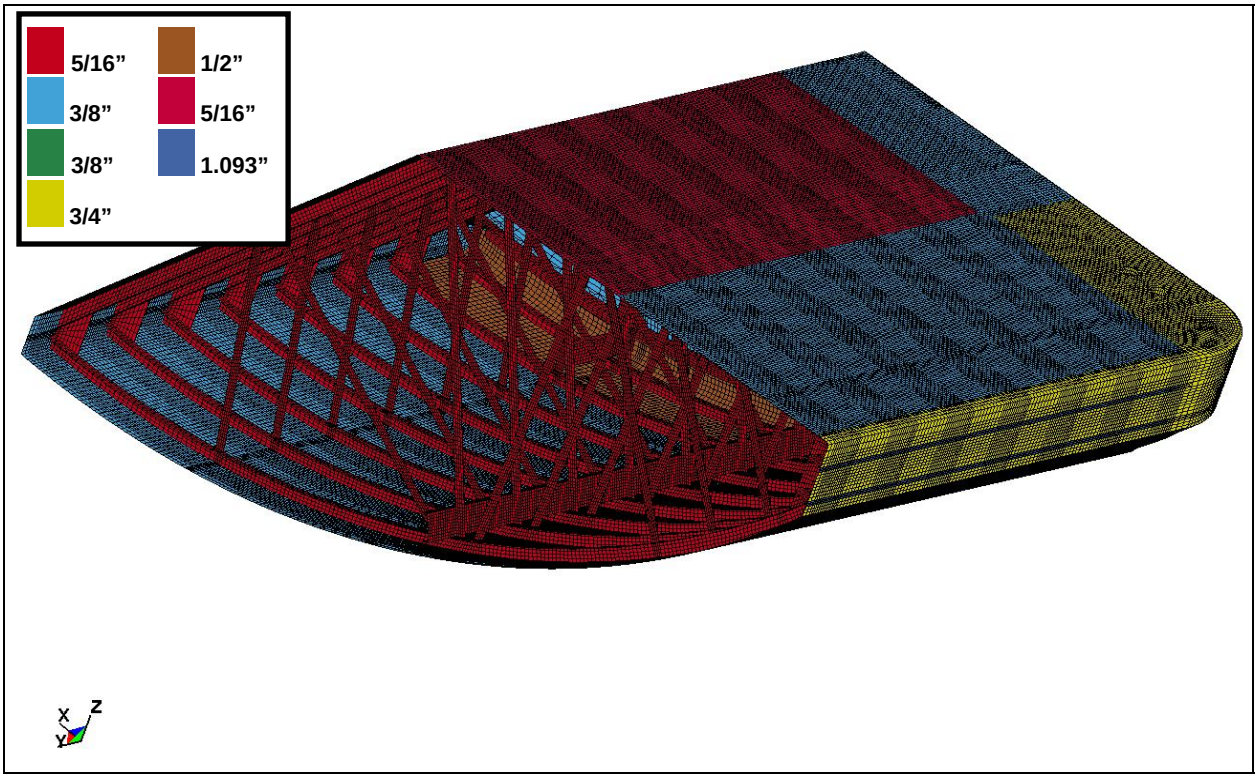

Figure 2.4. View of the bow of the barge at the centerline cut of the bow.

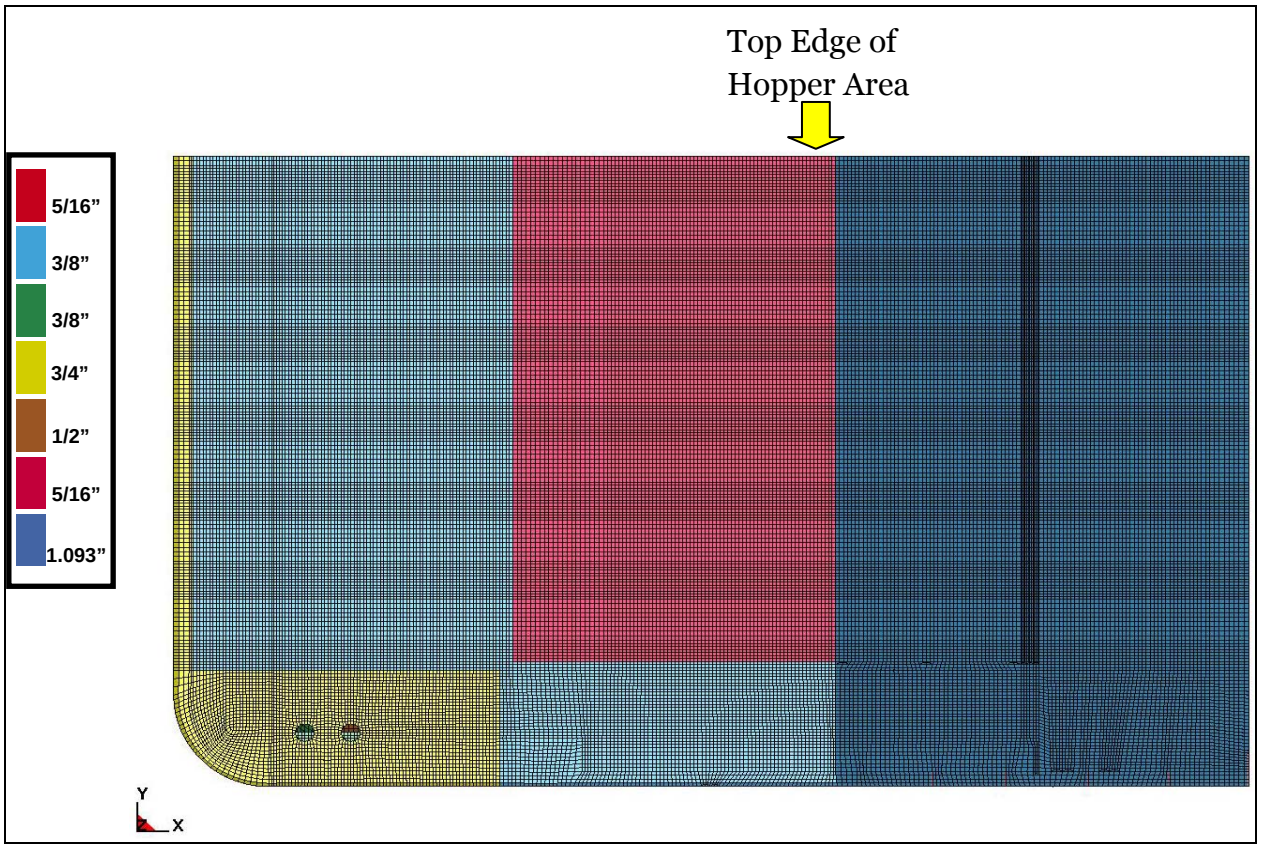

Figure 2.5. Overhead view of the bow of the barge.

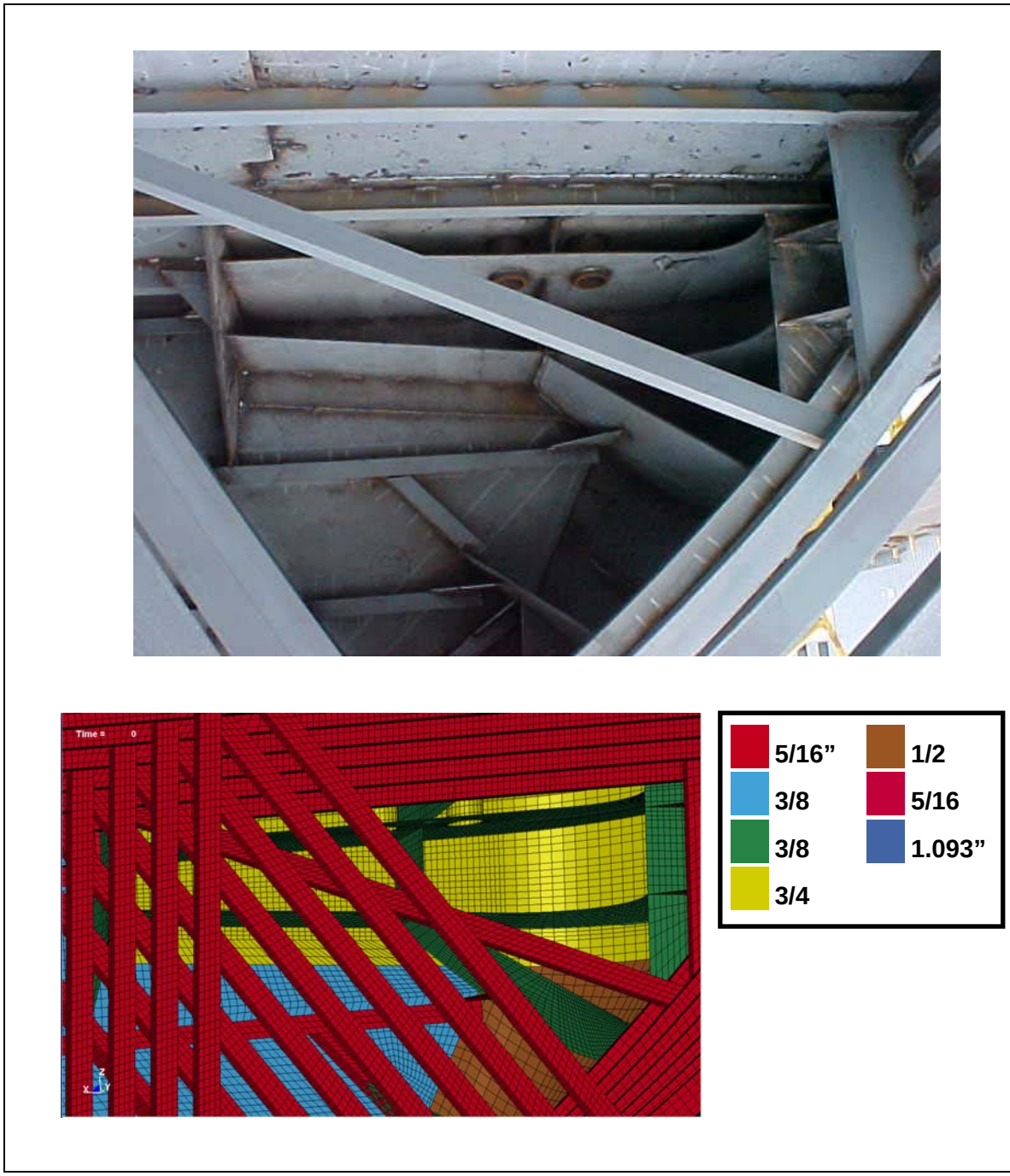

Figure 2.6. Internal views of the structural trusses and elliptical corner at the bow of the barge. (Top) Actual internal structural truss members and the elliptical corner. (Bottom) Corresponding finite element model and material zone steel members, identified by steel thicknesses.

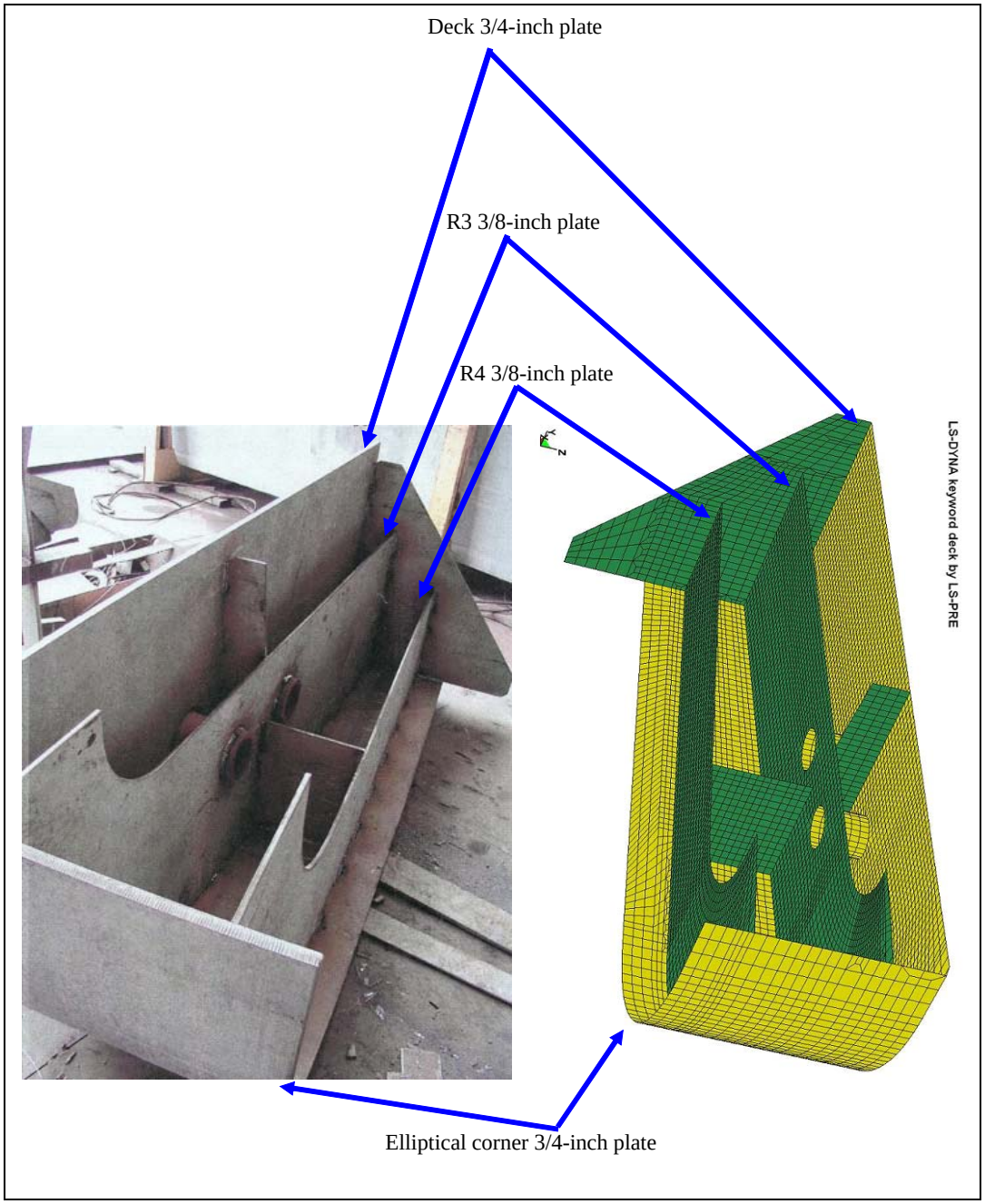

Figure 2.7. Views of the elliptical corner structural member. Interior view of the assemblage of the elliptical corner (left) resting on the ground from a bow point of view. (Right) Corresponding finite element model view.

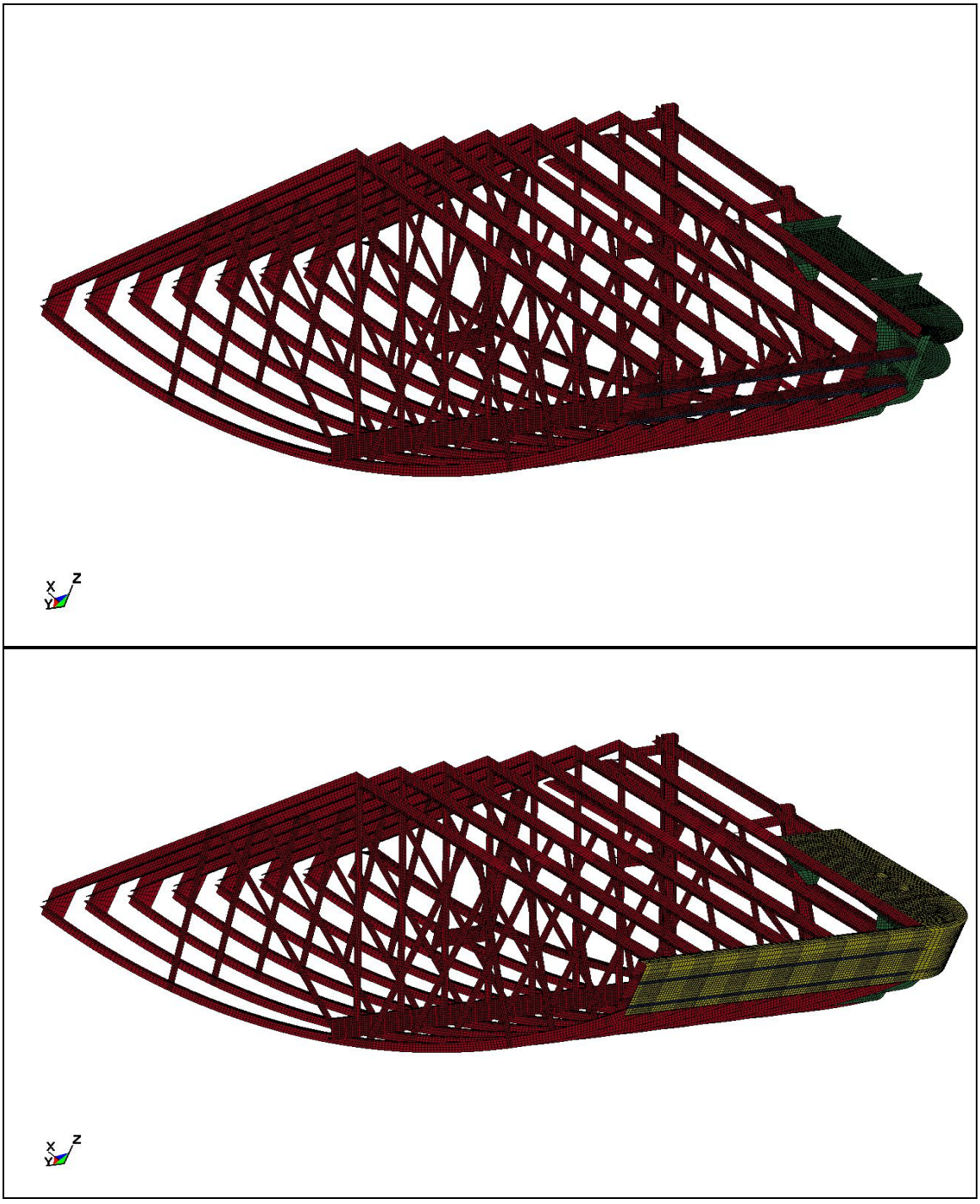

Figure 2.8. Internal structural members with the deck and hull plates removed.
(Top) Centerline/elevated view of internal members (elliptical corner plates in green on right).
(Bottom) Centerline/elevated view of internal members with three-quarter-inch-thick plate on elliptical corner and headlog.

2.3 Material modeling and material properties

With regard to material modeling used for the structural steel, significant yielding is expected to occur during crushing of the deck, hull plates, and the internal structural members in the impact corner zone of the bow. As such, all shell elements in the model of the bow were specified with a plastic-multilinear material model matching the stress-strain data derived from tests conducted on plate steel obtained for an actual barge. A large-displacement, large strain formulation was used for the shell elements in the LS-DYNA impact analyses. Therefore, the true (Cauchy) stress and true (logarithmic) strain data was used (Figure 2.9). This material model for A-36 steel was obtained from tests conducted at the University of Florida on standard 18-in. tension coupon (Consolazio et al. 2002). The steel model for A-36 steel has an initial yield of 36 kips/in.^{2} (2.48e + 08 N/m^2), a yield strain of 0.0012, and a failure strain of 0.2. In the LS-DYNA analyses, the material model was specified as an effective stress versus effective plastic strain, LS-DYNA material number 24, *MAT_PIECEWISE_LINEAR_PLASTICITY. Other material model parameters specified as input are:

- E = 30,000 ksi
- Poisson's ratio = 0.33
- Yield stress = 48 ksi
- Rupture stress = 86.6 ksi at 25% strain
- 20% plastic strain failure (i.e., EPPF).

Note that the rupture strain of 20% is specified in these LS-DYNA impact analyses. The implications are that when the strain reaches 20%, the strain integration point is removed from the analysis by LS-DYNA.

The LS-DYNA material number 24 model allows for the addition of strain rate effects on the material using the Cowper Symonds model. However, these simulations did not implement any strain rate effects for the A-36 steel material because the barge impact events are not high-speed impact simulations.

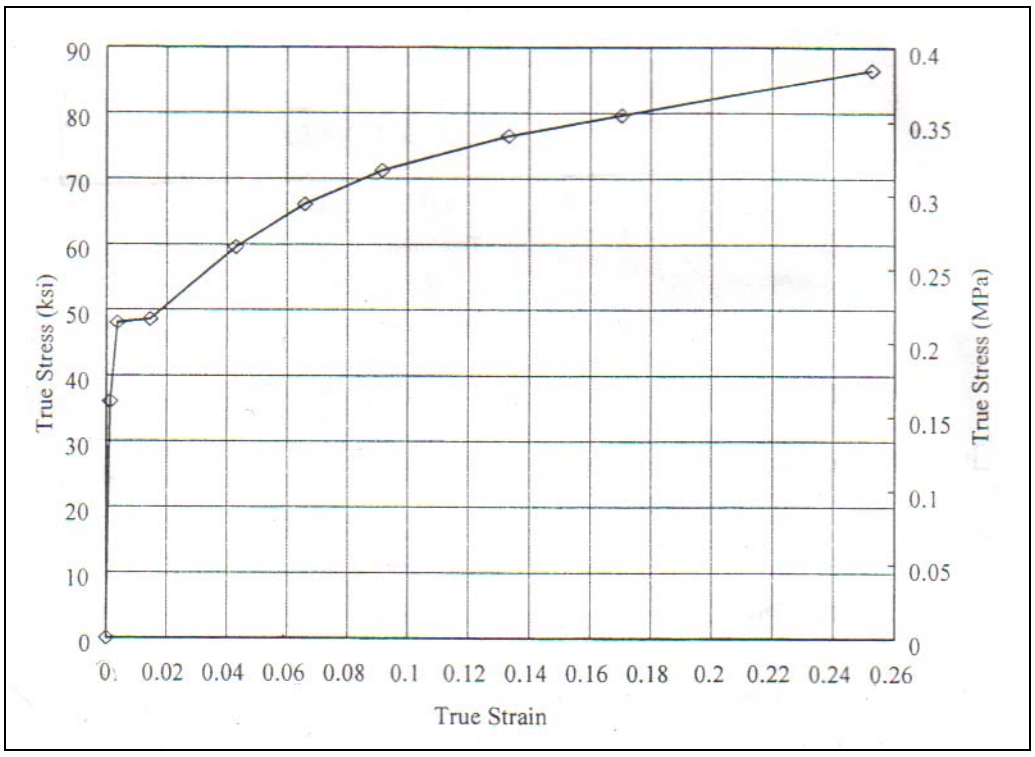

Figure 2.9. True stress versus true strain for A-36 structural steel (after Consolazio et al. 2002).

3 Limiting Impact Force Computations

3.1 Introduction

This chapter discusses the results of a series of 24 nonlinear finite element analyses using the 177,241 element mesh with the assigned A-36 steel material properties discussed in Chapter 2. The object of the nonlinear finite element analysis (using LS-DYNA) is to compute the limiting impact force due to yielding and buckling of the plates and internal structural framing at the impact corner of the barge during its glancing blow impact with a lock approach wall. Because the nonlinear deformations are concentrated in the front half of the bow region closest to the impact corner, only half of the jumbo open-hopper bow shown in Figure 2.1 is modeled in the analysis.

3.2 Nonlinear impact analyses

Lock approach walls are designed for usual, unusual, and extreme loads. The report "Barge Impact Analysis for Rigid Walls" (ETL 1110-2-563) provides a summary of the design requirements for these three load cases. The load cases are defined in terms of the annual probability of exceedance. The design information contained in the 2004 ETL report is summarized in Table 3.1. This information also includes ranges for nonsite-specific velocities (expressed in local barge coordinates) for the three load cases to use in preliminary analyses when site-specific traffic study results are not yet available.

Table 3.1. Three design load condition categories, frequency of loadings, and typical ranges for non-site-specific impact angles and approach velocities (from ETL 1110-2-563).

Load Condition	Annual Probability of Exceedance (Return Period)	Performance Criteria	Forward Velocity, V_x (ft/sec)	Lateral Velocity, V_y (ft/sec)	Approach Angle θ (°)
Usual	≥0.1 (1–10 years)	No damage	0.5–2.0	0.01–0.1	5–10
Unusual	<0.1 but >0.00333 (10–300 years)	Reparable damage	3.0–4.0	0.4–0.5	10–20
Extreme	<0.00333 (>300 years)	Noncollapse	4.0–6.0	<1.0	20–35

The velocity of a barge is usually specified in local barge coordinates as shown in Figure 3.1 and is a vector quantity. The velocity of a barge train is usually specified in the local barge axis; longitudinal (local "*x*" axis) and transverse (local "*y*" axis). In this case two velocities are specified, V_x and V_y. To obtain the velocity normal to the wall, an axis transformation equation is needed. This expression is the following:

$$\begin{Bmatrix} V_{par} \\ V_{norm} \end{Bmatrix} = [C]^{-1} \begin{Bmatrix} V_x \\ V_y \end{Bmatrix} \tag{3.1}$$

where $[C]^{-1} = \begin{bmatrix} \cos\theta & -\sin\theta \\ \sin\theta & \cos\theta \end{bmatrix}$, and V_{par} and V_{norm} are the velocity parallel (global "*X*" axis) and normal (global "*Y*" axis) to the wall, respectively. Equation 3.1 can be obtained easily from Figure 3.1.

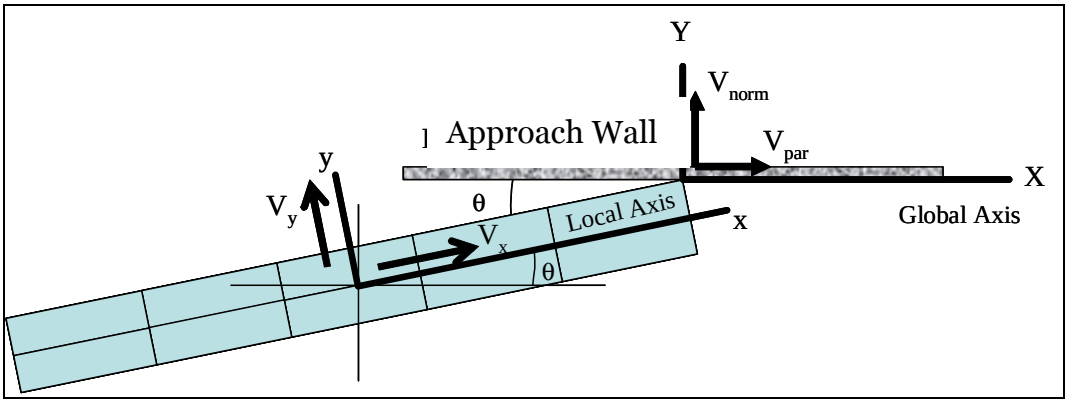

Figure 3.1. Velocity vector transformation, from local to global axis.

Using the minimum/maximum ranges in Table 3.1 for non-site-specific (1) impact (i.e., approach) angles, (2) forward velocities, and (3) lateral velocities for each of the three load cases, a combination of 24 sets of approach angles and velocities normal to the wall were derived. The results of these computations are summarized in Table 3.2, along with other data pertinent to the LS-DYNA analyses. This information served as the basis for the 24 LS-DYNA runs; run numbers are also included in this table.

Table 3.2. Twenty-four LS-DYNA runs.

Category	Impact Angle Θ (°)	Forward Velocity, V_x		Lateral Velocity, V_y		Approach Velocity, V			Normal Velocity		Parallel Velocity		Case No.
		(in./sec)	(ft/sec)	(in./sec)	(ft/sec)	(in./sec)	(ft/sec)	β (°)	(in./sec)	(ft/sec)	(in./sec)	(ft/sec)	
Usual	5	6	0.5	0.12	0.01	6.0012	0.5001	1.1458	0.6425	0.0535	5.9667	0.4972	1
Usual	5	6	0.5	1.2	0.1	6.1188	0.5099	11.3099	1.7184	0.1432	5.8726	0.4894	2
Usual	5	24	2	0.12	0.01	24.0003	2.	0.2865	2.2113	0.1843	23.8982	1.9915	3
Usual	5	24	2	1.2	0.1	24.03	2.0025	2.8624	3.2872	0.2739	23.8041	1.9837	4
Usual	10	6	0.5	0.12	0.01	6.0012	0.5001	1.1458	1.1601	0.0967	5.888	0.4907	5
Usual	10	6	0.5	1.2	0.1	6.1188	0.5099	11.3099	2.2237	0.1853	5.7005	0.475	6
Usual	10	24	2	0.12	0.01	24.0003	2.	0.2865	4.2857	0.3571	23.6145	1.9679	7
Usual	10	24	2	1.2	0.1	24.03	2.0025	2.8624	5.3493	0.4458	23.427	1.9523	8
Unusual	10	36	3	4.8	0.4	36.3186	3.0265	7.5946	10.9784	0.9149	34.6196	2.885	9
Unusual	10	36	3	6	0.5	36.4966	3.0414	9.4623	12.1602	1.0133	34.4112	2.8676	10
Unusual	10	48	4	4.8	0.4	48.2394	4.02	5.7106	13.0622	1.0885	46.4373	3.8698	11
Unusual	10	48	4	6	0.5	48.3735	4.0311	7.125	14.244	1.187	46.2289	3.8524	12
Unusual	20	36	3	4.8	0.4	36.3186	3.0265	7.5946	16.8232	1.4019	32.1872	2.6823	13
Unusual	20	36	3	6	0.5	36.4966	3.0414	9.4623	17.9509	1.4959	31.7768	2.6481	14
Unusual	20	48	4	4.8	0.4	48.2394	4.02	5.7106	20.9275	1.744	43.4635	3.622	15
Unusual	20	48	4	6	0.5	48.3735	4.0311	7.125	22.0551	1.8379	43.0531	3.5878	16
Extreme	20	48	4	7.2	0.6	48.537	4.0447	8.5308	23.1828	1.9319	42.6427	3.5536	17
Extreme	20	48	4	10.8	0.9	49.2	4.1	12.6804	26.5656	2.2138	41.4114	3.451	18
Extreme	20	72	6	7.2	0.6	72.3591	6.0299	5.7106	31.3912	2.6159	65.1953	5.4329	19
Extreme	20	72	6	10.8	0.9	72.8055	6.0671	8.5308	34.7741	2.8978	63.9641	5.3303	20
Extreme	35	48	4	7.2	0.6	48.537	4.0447	8.5308	33.4296	2.7858	35.1895	2.9325	21
Extreme	35	48	4	10.8	0.9	49.2	4.1	12.6804	36.3785	3.0315	33.1247	2.7604	22
Extreme	35	72	6	7.2	0.6	72.3591	6.0299	5.7106	47.1954	3.9329	54.8492	4.5708	23
Extreme	35	72	6	10.8	0.9	72.8055	6.0671	8.5308	50.1443	4.1787	52.7843	4.3987	24

There are four approach (i.e., impact) angles used in the 24 nonlinear finite element analyses: 5°, 10°, 20°, and 35°. The velocity normal to the approach wall varies from a low of 0.64 in./sec (0.054 ft/sec) to a high value of 50.1 in./sec (4.18 ft/sec). The authors of this report consider these barge impact problems to be low-velocity impacts, compared to "crash" analyses involving the impacts between vehicles and highway barriers.[1] Each of the 24 LS-DYNA analyses is conducted using the *RIGIDWALL_GEOMETRIC_FLAT_MOTION option. The barge bow mesh is fixed in space (with zero displacement boundary conditions specified along the centerline and the hopper) with the appropriate approach angle θ (Table 3.2) between the side of the barge and the side of the approach wall (see Figure 3.1) for the run under study. The flat nonpenetrating rigid wall is brought into contact with the barge at a constant normal velocity as listed in Table 3.2 for that particular run until 36 in. of penetration by the "rigid" (approach) wall into the barge mesh is accomplished. The LS-DYNA contact surface option *CONTACT_AUTOMATIC_SINGLE_SURFACE is engaged in these analyses. A coefficient of friction equal to 0.6 (appropriate for steel barge on steel armor on the approach wall)[2] is specified for the contact surface between the "rigid" wall and the barge. The contact force between the approach wall and the barge that is being "crushed" at the impact corner region of the bow is monitored throughout the analysis. The nonlinear material model allows for a nonlinear structural system response of the multi-degree-of-freedom structural system that is the barge bow.

3.3 Results

This section summarizes the computed results for the 24 nonlinear finite element analyses. The deck, the hull and internal plates, and the internal structural members all develop elastic and then plastic strains within the steel members as the "rigid" wall contacts the barge corner and then displaces the corner.

---

[1] Bathe et al. (1999) observe that crash analyses simulate fast phenomena requiring a transient analysis whereas crush analyses simulate slow phenomena that are approximately analyzed using static analysis procedures or implicit dynamic techniques. In recent years, Dr. Gary R. Consolazio and his students have been using numerical methods to quantify barge impact loads on bridges for head-on collisions with bridge piers (e.g., Consolazio et al. 2002; Consolazio and Cowan 2003). These calculations have involved the use of the general purpose, nonlinear finite element computer programs ADINA and LS-DYNA. Their LS-DYNA models and analyses share many common modeling and analysis features with those discussed in this report.

[2] Sullivan (1988); Encarta Encyclopedia (2004); Grigoriev et al. (1997).

Figure 1.4 shows the overhead views of the barge impact corner at initial contact with the wall and after 36 in. of penetration for Case No. 9. Case No. 9 is for the unusual loading condition with an approach angle of 10°. Figure 1.5 shows the force normal to the approach wall versus displacement of the impact corner for this case. This force represents both the normal contact force applied to the approach wall as well as the force imparted by the wall onto the multi-degree-of-freedom structural system of the barge. The normal force (Figure 1.5) ranges in value from 0 kips to a maximum force of 3,497 kips at 4.8 in. of permanent normal deformation at the impact corner. The Case No. 9 LS-DYNA analysis continued until there was 36 in. of permanent deformation of the rigid wall into the impact corner region of the barge. The nonlinearity in Figure 1.5 results from (1) the nonlinear true-stress versus true-strain relationship for A-36 steel (Figure 2.9), and (2) the removal of strain integration points and elements when an effective plastic strain of 20% is achieved within the shell elements used to model the structural members and plates during the course of the "crushing" analysis of the elliptical corner.

Figure 3.2 shows the distribution of effective plastic strain at a permanent deformation of 4.8 in. at the impact corner of the bow for Case No. 9. Note the "crease" or standing wave of deformation in the deck plate in the upper right figure as well as the "dimpling" of the elliptical corner at this level of deformation. Figure 3.3 shows a close-up view of the distribution of effective plastic strain at the impact corner (i.e., the elliptical corner). Note the erosion (i.e., removal) of elements (by LS-DYNA) at the intersection of the deck with the elliptical corner; this results from an effective plastic strain of 0.2 (i.e., 20%) being achieved by shell elements within this zone. Figure 3.4 shows the distribution of von Mises stress at a permanent deformation of 4.8 in. at the impact corner of the bow for Case No. 9.

Figure 3.5 shows the distribution of effective plastic strain at a permanent deformation of 36 in. at the impact corner of the bow for Case No. 9. Note that at this level of permanent deformation the multiple "creases" or standing waves of deformation in the deck plate in the upper right figure as well as the "crushing" of the elliptical corner at 36 in. of deformation. Figure 3.6 shows a close-up view of the distribution of effective plastic strain at the impact corner (i.e., the elliptical corner). Note the erosion (i.e., removal) of elements at the intersection of the deck with the elliptical corner as a result of an effective plastic strain of 0.2 (i.e., 20%) being

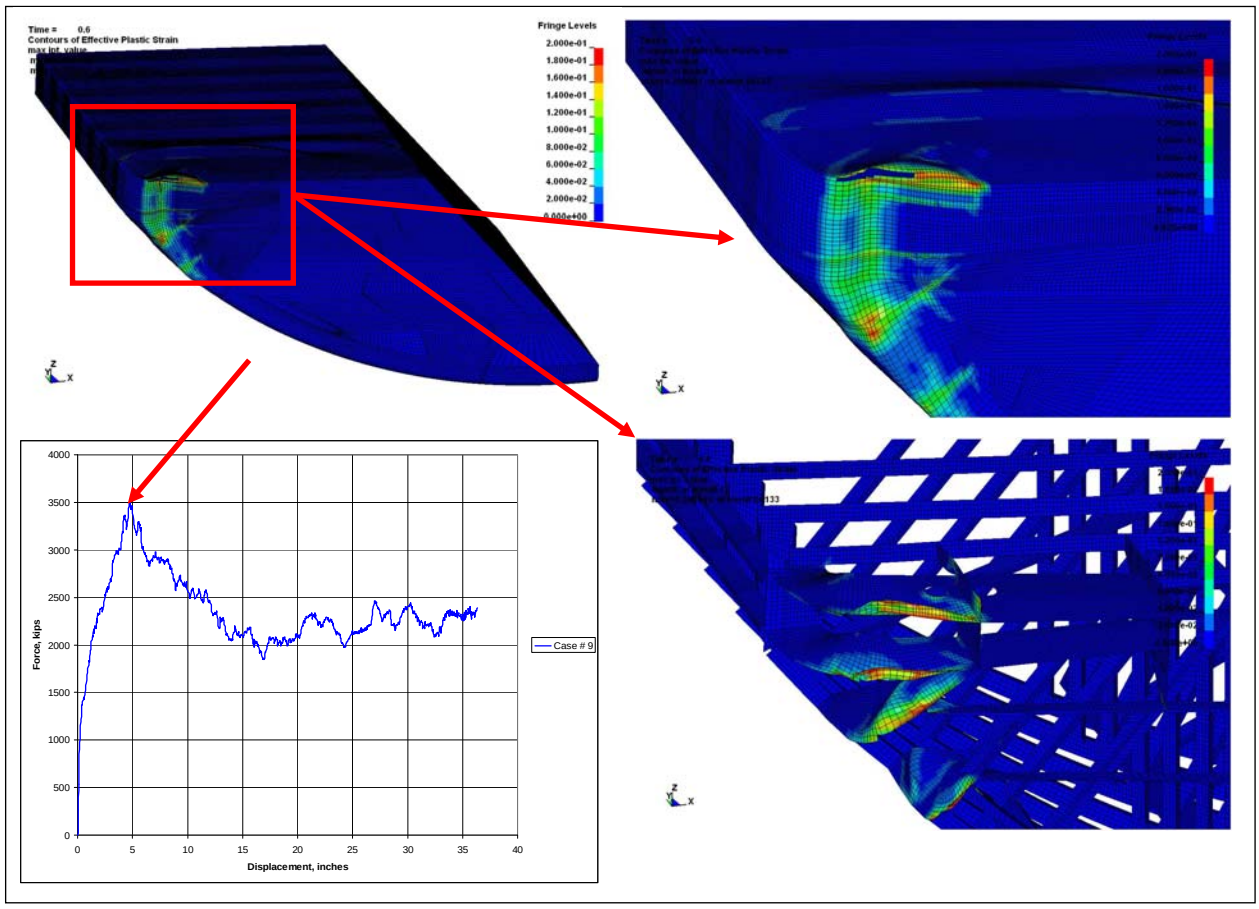

Figure 3.2. Distribution of effective plastic strain (in decimal fraction) at 4.8 in. permanent deformation and force versus displacement plot of the bow and impact corner for Case No. 9. Unusual loading condition with an approach angle of 10°.

achieved in this zone. Figure 3.7 shows the distribution of von Mises stress at a permanent deformation of 36 in. at the impact corner of the bow for Case No. 9. Due to the nonlinear material response and the erosion of elements, the normal force at 36 in. of permanent deformation shown in Figure 1.5 is approximately 2,300 kips, a significant reduction from the maximum force of 3,495 kips at 4.8 in. of permanent normal deformation at the impact corner.

Figures 3.8–3.13 summarize the force normal to the wall versus displacement for the 24 LS-DYNA Cases. The computations are made for 0-36 in. of permanent deformation normal to the wall within the barge impact corner region. The 24 cases in Table 3.2 are presented in groups of four per figure, with each figure sharing a common load case (i.e., usual, unusual, or extreme) and common approach angle (i.e., impact angle).

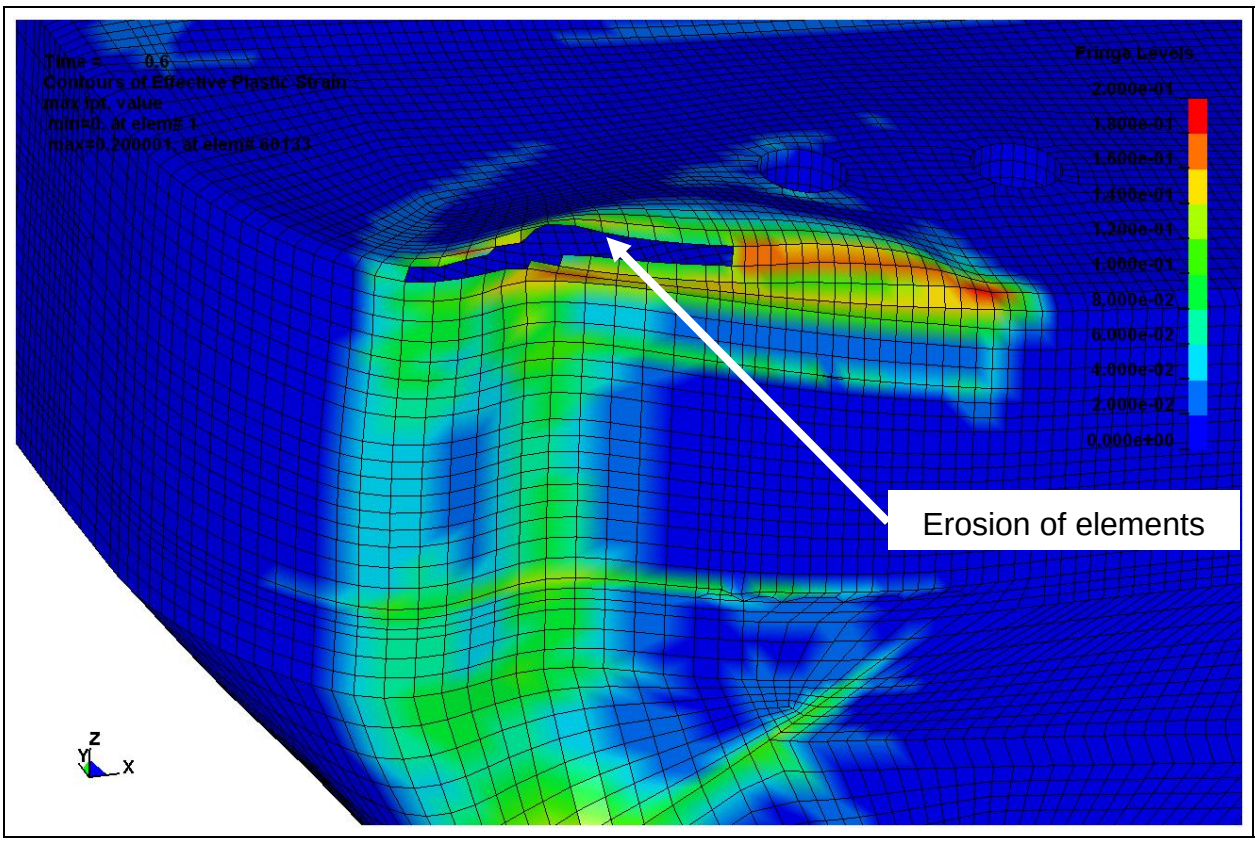

Figure 3.3. Distribution of effective plastic strain (in decimal fraction) at 4.8 in. permanent deformation and erosion of elements at the impact corner for Case No. 9. Unusual loading condition with an approach angle of 10°.

Figure 3.8 shows the force versus displacement of the impact corner for Cases Nos. 1–4 for a usual loading condition with an approach angle (i.e., impact angle) of 5°. The force versus displacement results up to and through the peak range from 3,360 to 3,605 kips. The peak force increases as the velocity normal to the wall increases. These four analyses tend to track each other up to 10 in. of permanent deformation before there is a noticeable divergence in results. After about 6 in. of permanent deformation, there is a significant drop-off in force with additional deformation, reflecting the nonlinear material response as well as the erosion of elements.

Figure 3.9 shows the force versus displacement of the impact corner for Case Nos. 5–8 for a usual loading condition with an approach angle (i.e., impact angle) of 10°. The force versus displacement results up to and through the first peak (of 3,250–3,410 kips) are nearly identical, with Case No. 5 diverging a little more from the others. These four analyses tend to track each other up to approximately 18 in. of permanent deformation

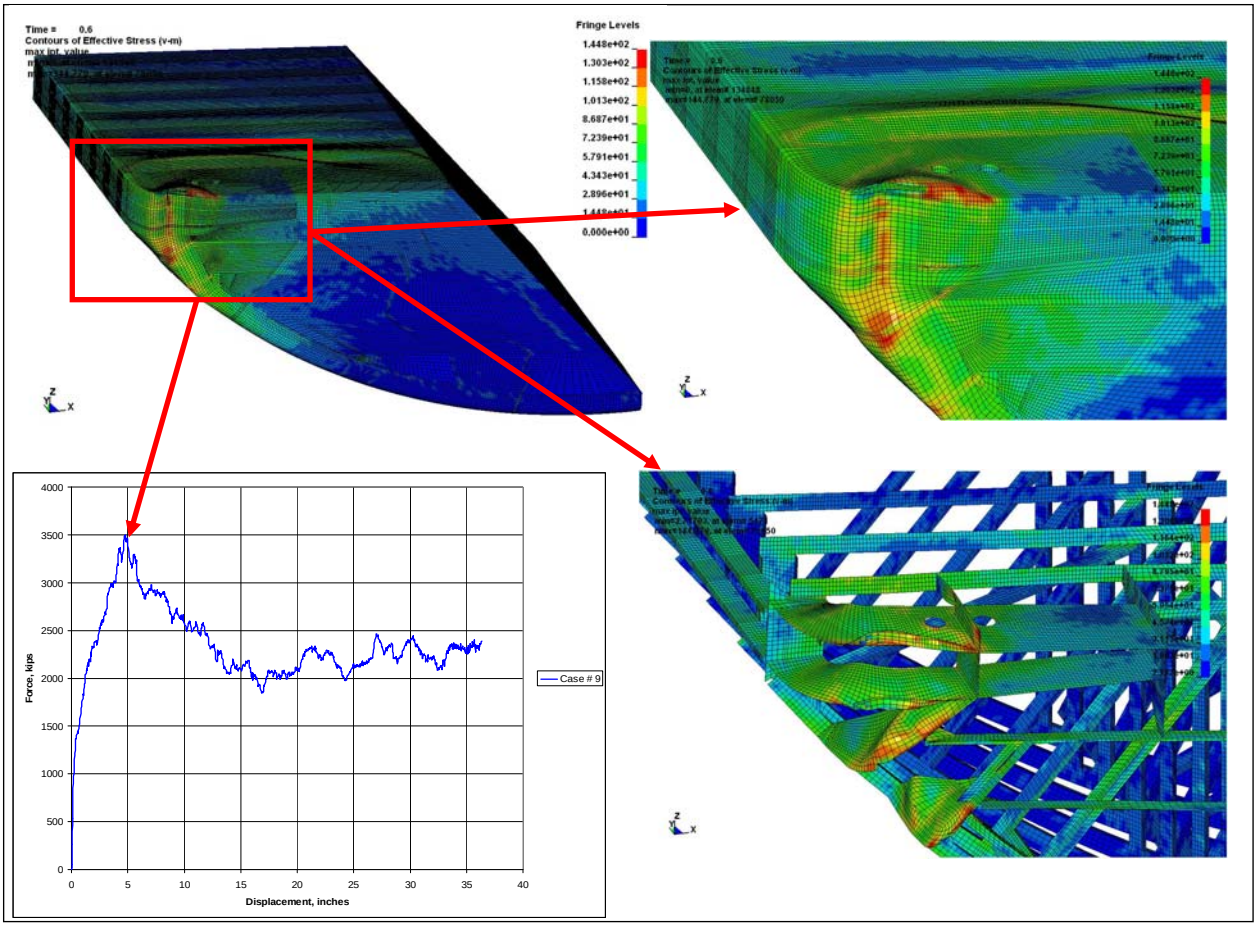

Figure 3.4. Distribution of von Mises stress at 4.8 in. permanent deformation and force versus displacement plot of the impact corner for Case No. 9. Unusual loading condition with an approach angle of 10°.

before there is a noticeable divergence in results. After about 6 in. of permanent deformation there is a significant drop-off in force with additional deformation; this reflects the nonlinear material response as well as the erosion of elements. The authors of this report again observe that there seems to be a dependence of the nonlinear response on the (normal) velocity specified in the analysis for this second set of four analyses. Specifically, Case No. 5 seems to diverge more from a general trend at the extremely large deformation of 27 in. It cannot be understated that there is significant plastic response and erosion of elements at this stage of the nonlinear analysis and the computations may be sensitive to small changes in plastic responses and element erosion during the course of nonlinear analyses of the multi-degree-of-freedom structural barge bow system. The end result in a nonlinear analysis depends upon the path taken.

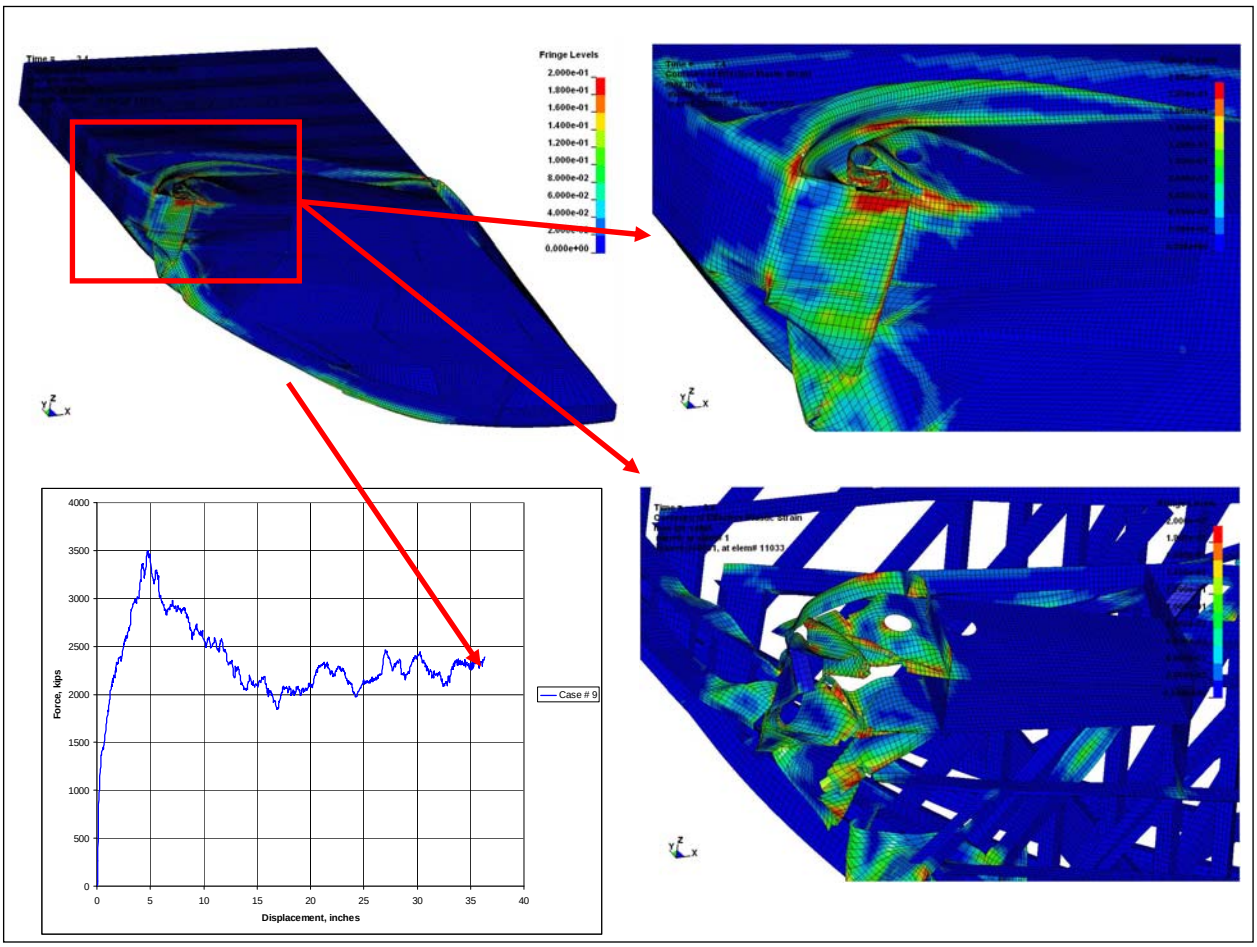

Figure 3.5. Distribution of effective plastic strain (in decimal fraction) at 36 in. permanent deformation and force versus displacement plot of the bow and impact corner for Case No. 9. Unusual loading condition with an approach angle of 10°.

Figure 3.10 shows the force versus displacement of the impact corner for Case Nos. 9–12 for an unusual loading condition with an approach angle (i.e., impact angle) of 10°. The force versus displacement results up to and through the first peak (of 3,450–3,500 kips) are identical. The magnitude of this first peak is only slightly greater than that computed for Case Nos. 5–8 (Table 3.3), which also has an approach angle of 10°. These four analyses tend to track each other up to approximately 20 in. of permanent deformation before there is a slight divergence in results. After about 5 in. of permanent deformation, there is a significant drop-off in force with additional deformation; this reflects the nonlinear material response as well as the erosion of elements. The authors of this report again observe that there seems to be a dependence of the nonlinear response on the (normal) velocity specified in the analysis for this third set of four analyses but with less divergence than observed in the previous eight case numbers.

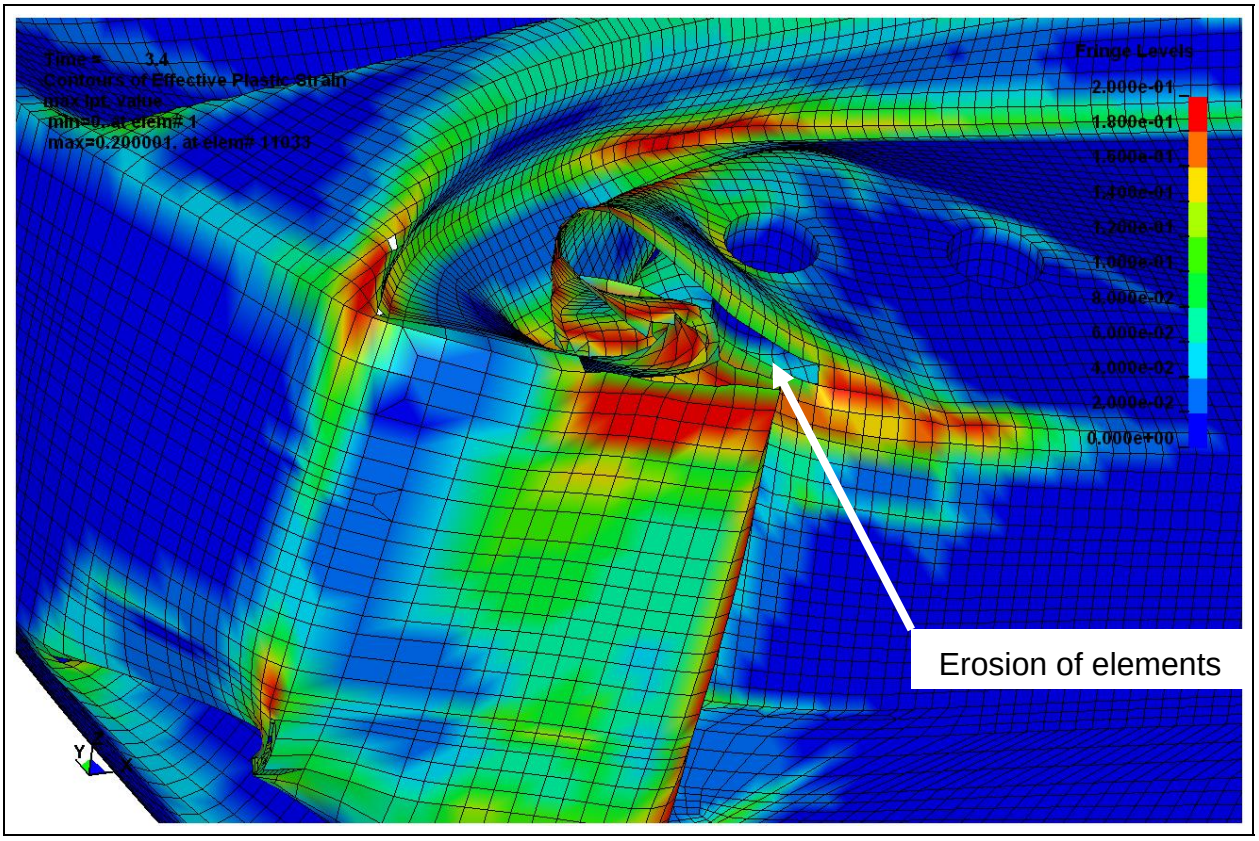

Figure 3.6. Distribution of effective plastic strain (in decimal fraction) at 36 in. permanent deformation and erosion of elements at the impact corner for Case No. 9. Unusual loading condition with an approach angle of 10°

Figure 3.11 shows the force versus displacement of the impact corner for Case Nos. 13–16 for an unusual loading condition with an approach angle (i.e., impact angle) of 20°. The force versus displacement results up to and through the first peak (of 3,180–3,390 kips) are identical. The magnitude of this first peak is a bit lower than that computed for Case Nos. 9–12 (Table 3.3), which has a smaller approach angle of 10°. These four analyses tend to track each other up to approximately 25 in. of permanent deformation before there is a slight divergence in results, with Case No. 13 showing more of a deviation among the four analyses. After about 10 in. of permanent deformation there is a significant drop-off in force with additional deformation; this reflects the nonlinear material response as well as the erosion of elements for this fourth set of cases. The authors of this report again observe that there seems to be a dependence of the nonlinear response on the (normal) velocity specified in the analysis for this fourth set of four analyses and with about the same level of divergence as observed in Case Nos. 9–12.

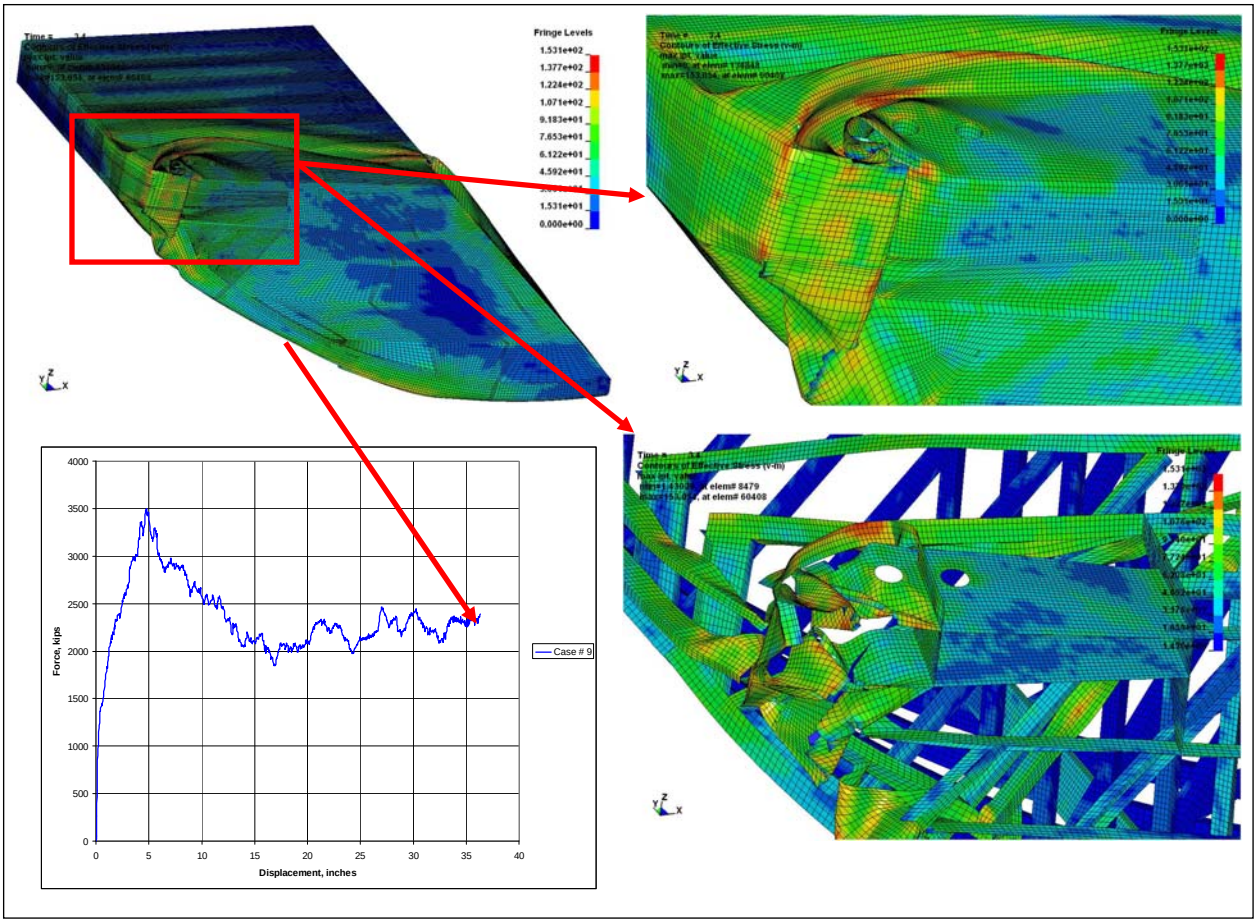

Figure 3.7. Distribution of von Mises stress at 36 in. permanent deformation and force versus displacement plot of the impact corner for Case No. 9. Unusual loading condition with an approach angle of 10°.

Figure 3.12 shows the force versus displacement of the impact corner for Case Nos. 17–20 for an extreme loading condition with an approach angle (i.e., impact angle) of 20°. The force versus displacement results up to and through the first peak (of 3,420–3,670 kips) follow the same general trend. The magnitude of this first peak is slightly higher than that computed for Case Nos. 13–16 (Table 3.3), which has the same approach angle of 20°. These four analyses tend to track each other through to 36 in. of permanent deformation, with Case No. 20 showing more of a deviation among the four analyses. Past about 11 in. of permanent deformation, there is a significant drop-off in force with additional deformation; this reflects the nonlinear material response as well as the erosion of elements for this fifth set of cases. The authors of this report again observe that there seems to be a dependence of the nonlinear response on the (normal) velocity specified in the analysis for this fifth set of four analyses.

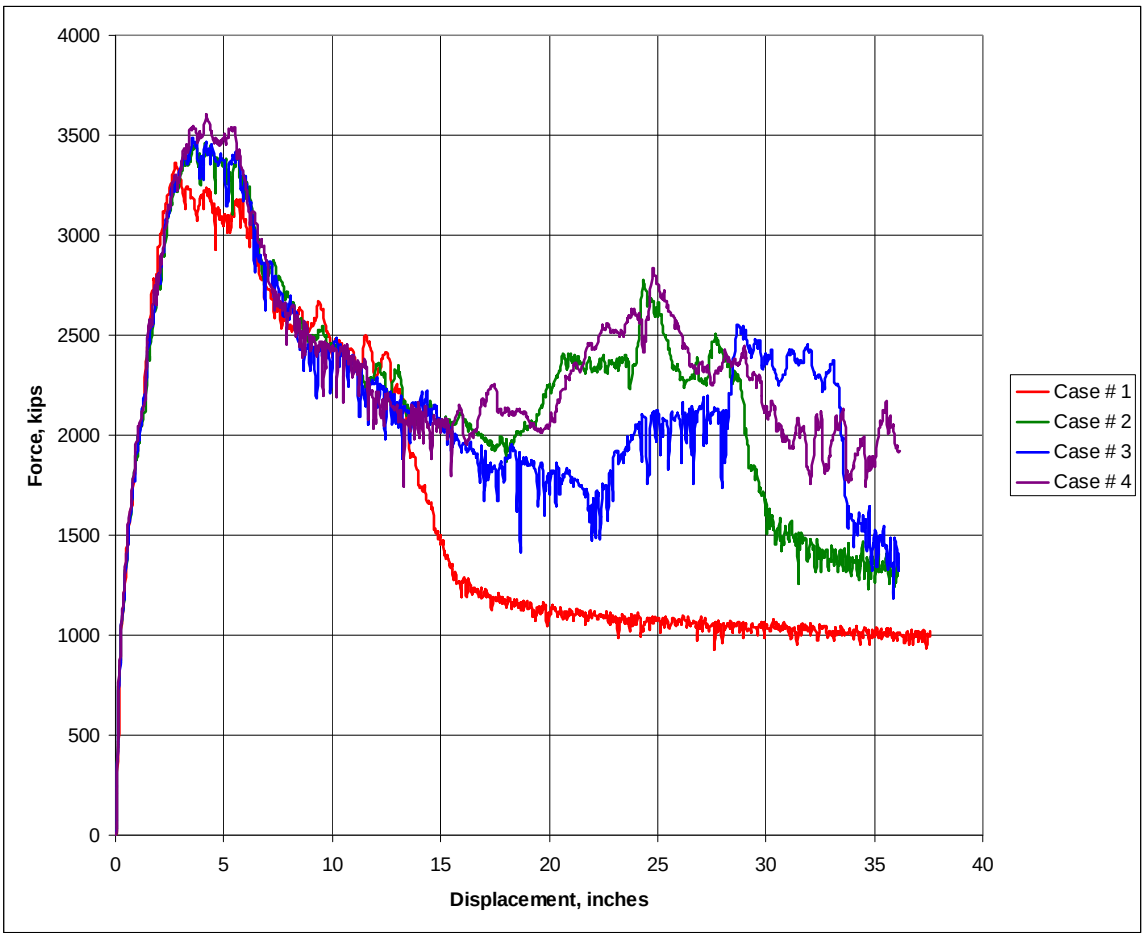

Figure 3.8. Force versus displacement of the impact corner for Case Nos. 1–4. Usual loading condition with an approach angle of 5°.

Figure 3.13 shows the force versus displacement of the impact corner for Case Nos. 21–24 for an extreme loading condition with an approach angle (i.e., impact angle) of 35°. The force versus displacement results follow the same general trend up to about 6 in. From 6 in. through to the first peak (of 3,170–3,910 kips) there is a dependency on the magnitude of the specified velocity normal to the approach wall; with the higher the normal velocity resulting in the higher peak force. Case Nos. 23 and 24 result in the highest peak forces among the 24 analyses (Table 3.3).

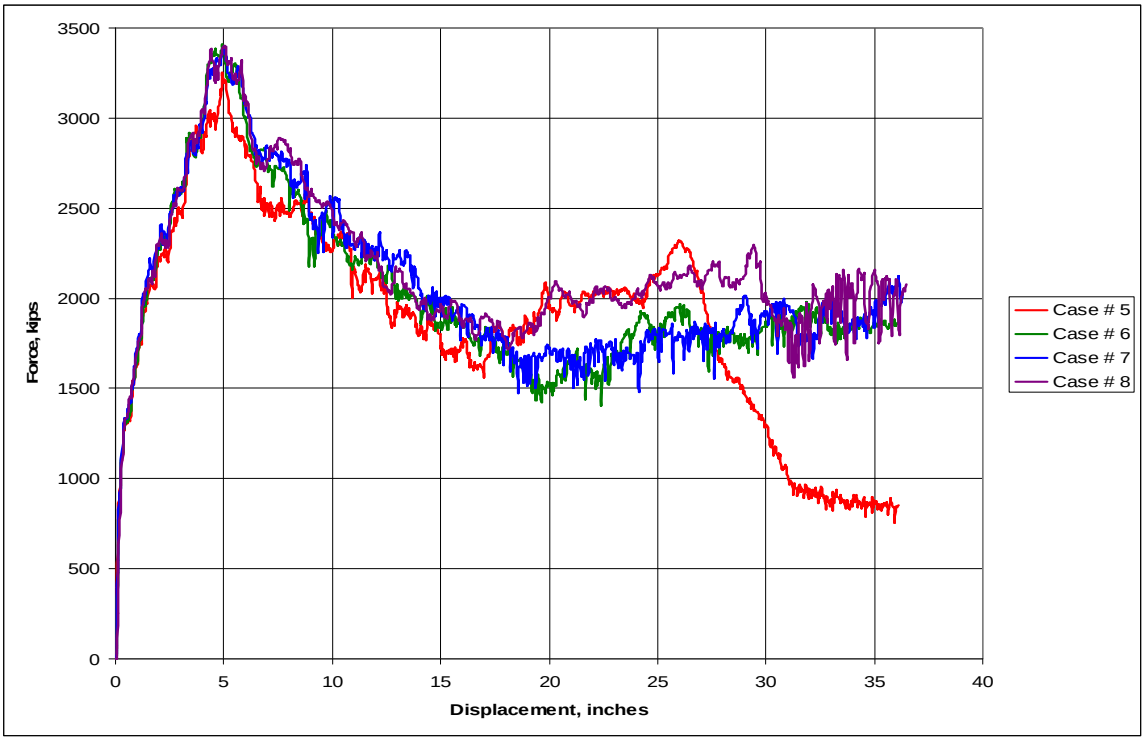

Figure 3.9. Force versus displacement of the impact corner for Case Nos. 5–8. Usual loading condition with an approach angle of 10°.

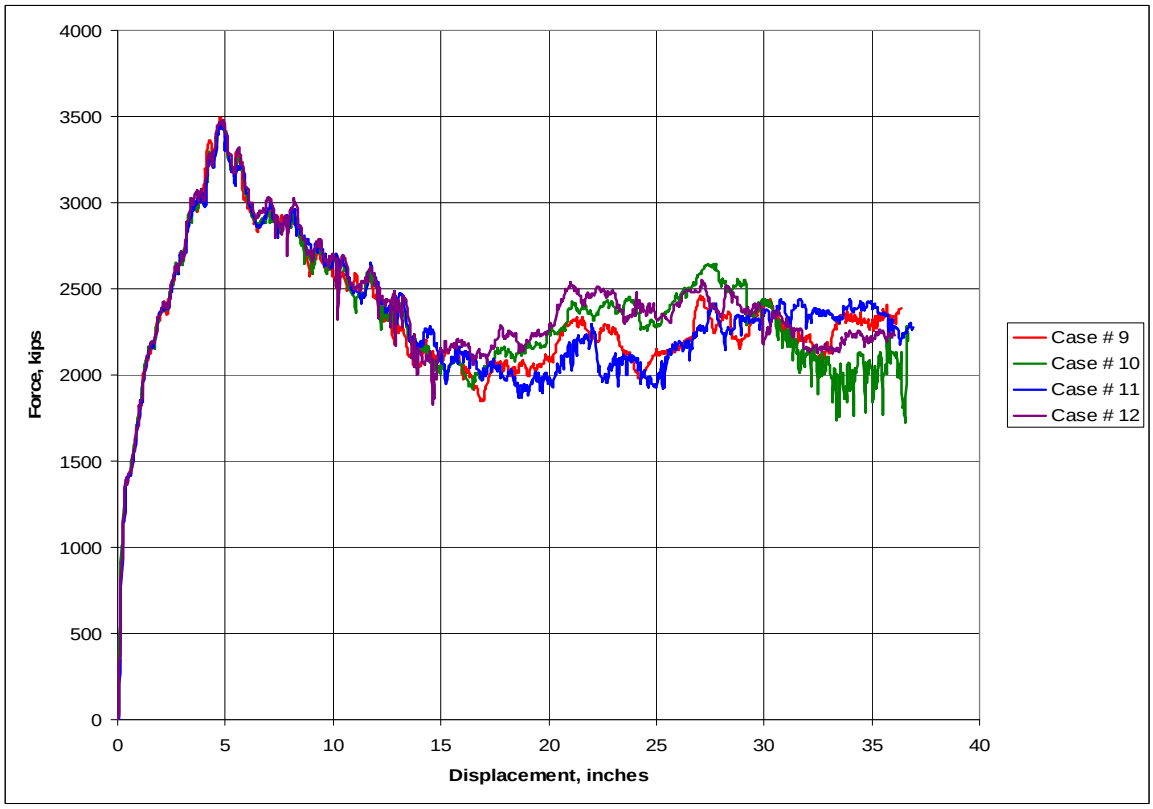

Figure 3.10. Force versus displacement of the impact corner for Case Nos. 9–12. Unusual loading condition with an approach angle of 10°.

Table 3.3. Summary of computed maximum force values for the 24 LS-DYNA runs.

Category	Impact Angle Θ (°)	Forward Velocity, V_x		Lateral Velocity, V_y		Approach Velocity, V			Normal Velocity		Maximum Force		Case No.
		(inch/sec)	(ft/sec)	(inch/sec)	(ft/sec)	(inch/sec)	(ft/sec)	β (°)	(inch/sec)	(ft/sec)	Force (kips)	Displacement (inch)	
Usual	5	6	0.5	0.12	0.01	6.0012	0.5001	1.1458	0.6425	0.0535	3361	2.78	1
Usual	5	6	0.5	1.2	0.1	6.1188	0.5099	11.3099	1.7184	0.1432	3463	3.71	2
Usual	5	24	2	0.12	0.01	24.0003	2.	0.2865	2.2113	0.1843	3484	3.57	3
Usual	5	24	2	1.2	0.1	24.03	2.0025	2.8624	3.2872	0.2739	3603	4.2	4
Usual	10	6	0.5	0.12	0.01	6.0012	0.5001	1.1458	1.1601	0.0967	3251	4.94	5
Usual	10	6	0.5	1.2	0.1	6.1188	0.5099	11.3099	2.2237	0.1853	3410	4.94	6
Usual	10	24	2	0.12	0.01	24.0003	2.	0.2865	4.2857	0.3571	3387	5.	7
Usual	10	24	2	1.2	0.1	24.03	2.0025	2.8624	5.3493	0.4458	3402	5.02	8
Unusual	10	36	3	4.8	0.4	36.3186	3.0265	7.5946	10.9784	0.9149	3497	4.78	9
Unusual	10	36	3	6	0.5	36.4966	3.0414	9.4623	12.1602	1.0133	3452	4.72	10
Unusual	10	48	4	4.8	0.4	48.2394	4.02	5.7106	13.0622	1.0885	3474	4.85	11
Unusual	10	48	4	6	0.5	48.3735	4.0311	7.125	14.244	1.187	3478	4.93	12
Unusual	20	36	3	4.8	0.4	36.3186	3.0265	7.5946	16.8232	1.4019	3177	9.93	13
Unusual	20	36	3	6	0.5	36.4966	3.0414	9.4623	17.9509	1.4959	3248	9.92	14
Unusual	20	48	4	4.8	0.4	48.2394	4.02	5.7106	20.9275	1.744	3373	9.8	15
Unusual	20	48	4	6	0.5	48.3735	4.0311	7.125	22.0551	1.8379	3390	9.87	16
Extreme	20	48	4	7.2	0.6	48.537	4.0447	8.5308	23.1828	1.9319	3415	9.87	17
Extreme	20	48	4	10.8	0.9	49.2	4.1	12.6804	26.5656	2.2138	3518	9.82	18
Extreme	20	72	6	7.2	0.6	72.3591	6.0299	5.7106	31.3912	2.6159	3552	9.88	19
Extreme	20	72	6	10.8	0.9	72.8055	6.0671	8.5308	34.7741	2.8978	3674	10.87	20
Extreme	35	48	4	7.2	0.6	48.537	4.0447	8.5308	33.4296	2.7858	3174	13.01	21
Extreme	35	48	4	10.8	0.9	49.2	4.1	12.6804	36.3785	3.0315	3405	13.82	22
Extreme	35	72	6	7.2	0.6	72.3591	6.0299	5.7106	47.1954	3.9329	3872	14.29	23
Extreme	35	72	6	10.8	0.9	72.8055	6.0671	8.5308	50.1443	4.1787	3906	14.19	24

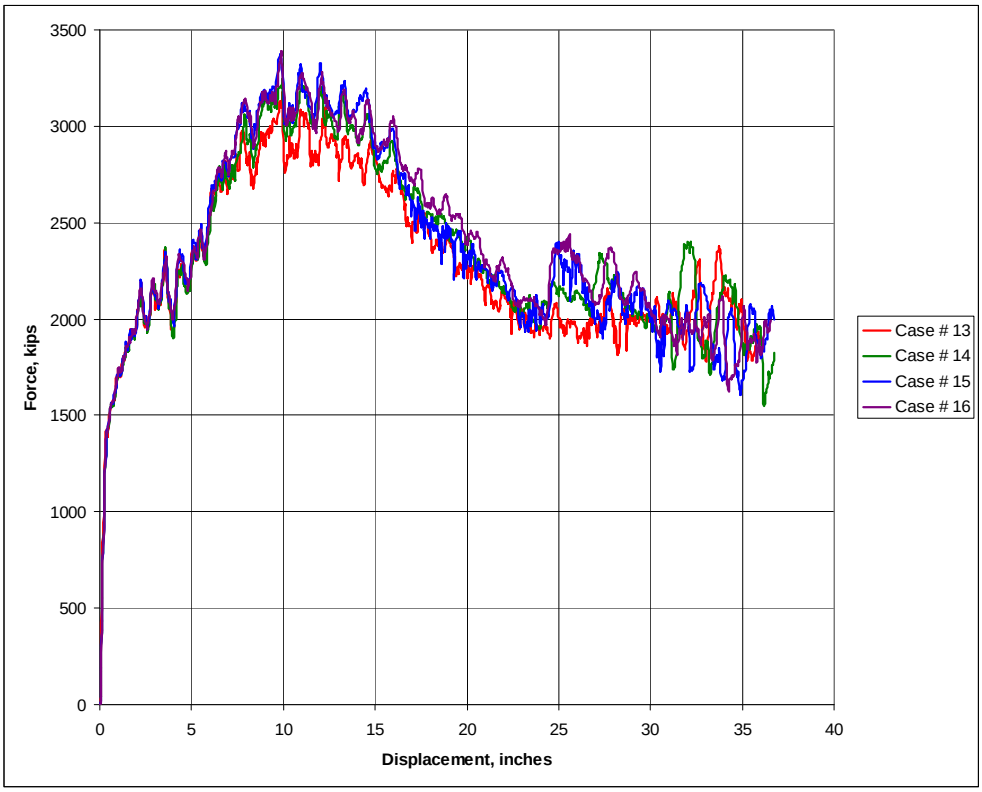

Figure 3.11. Force versus displacement of the impact corner for Case Nos. 13–16. Unusual loading condition with an approach angle of 20°.

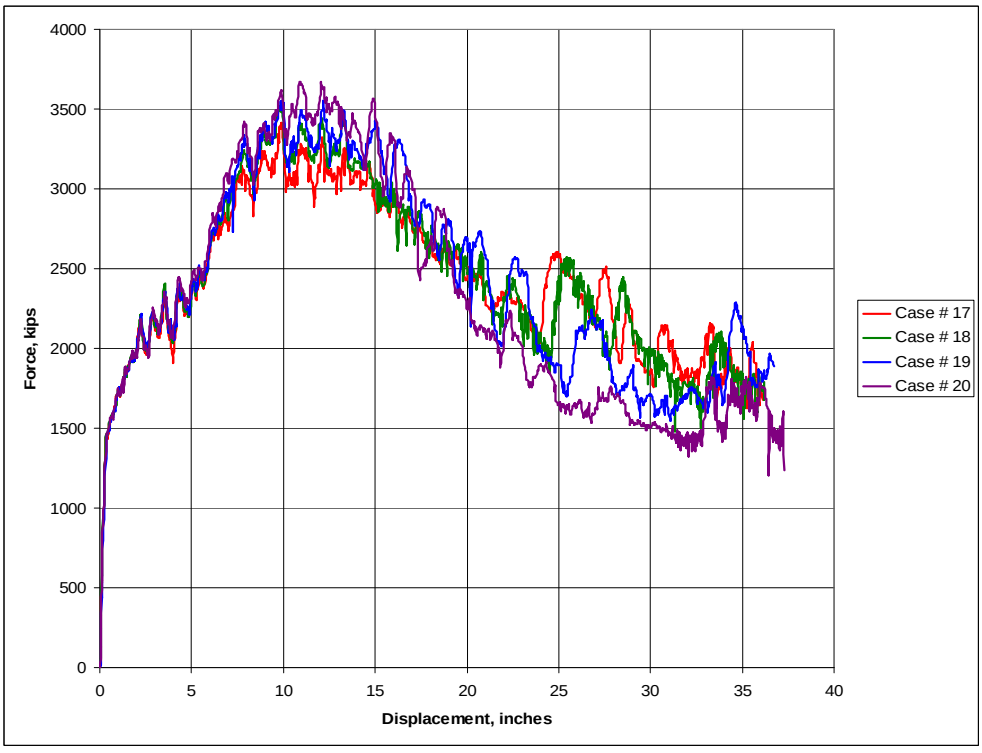

Figure 3.12. Force versus displacement of the impact corner for Case Nos. 17–20. Extreme loading condition with an approach angle of 20°.

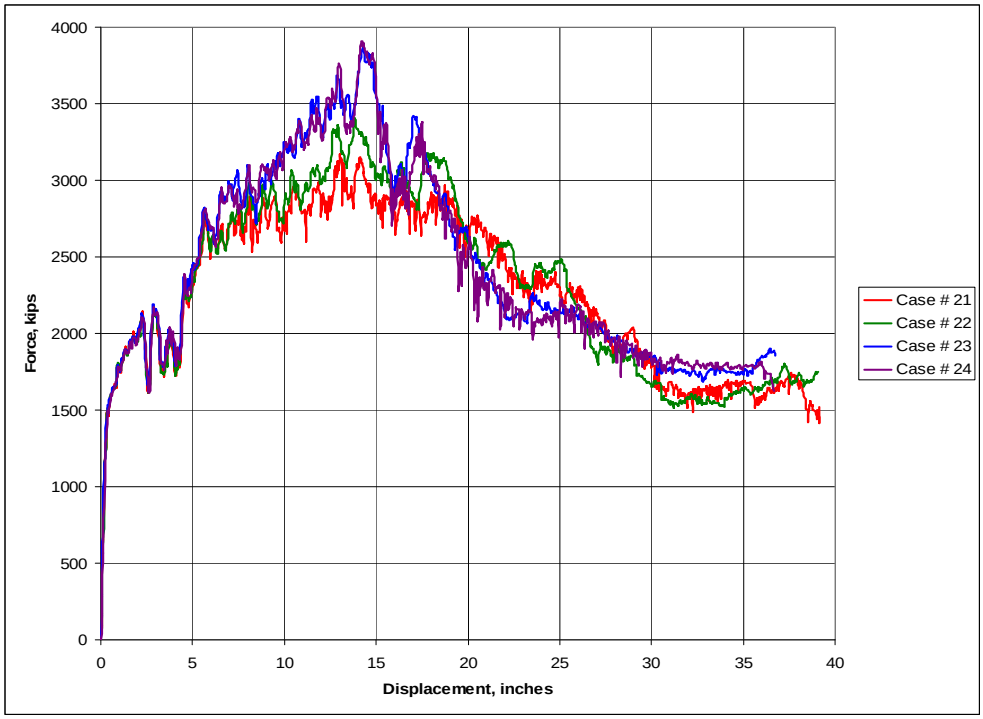

Figure 3.13. Force versus displacement of the impact corner for Case Nos. 21–24. Extreme loading condition with an approach angle of 35°.

Case Nos. 21 and 22 tend to track one another, whereas Case Nos. 23 and 24 track one another. All four analyses tend to follow the same general pattern out to 36 in. of permanent deformation; after 14–15 in. of permanent deformation there is a significant drop-off in force with additional deformation, reflecting the nonlinear material response as well as the erosion of elements for this sixth set of cases. The authors of this report again observe that there seems to be a dependence of the nonlinear response on the (normal) velocity specified in the analysis for this sixth set of four analyses.

4 Summary, Results, and Conclusions

4.1 Summary

This research report discusses the results of a series of 24 nonlinear finite element analysis (using LS-DYNA) to compute the limiting impact force due to the yielding and buckling of plates and internal structural framing at the impact corner of the barge during its glancing blow impact with a lock approach wall. A finite element mesh of the front half of the bow of a jumbo open-hopper barge consisting of 179,238 nodes and 177,241 elements was constructed. Because of the localization of the nonlinear response during impact of the bow of the barge with the approach wall, only the bow region of the jumbo open-hopper barge (Figure 2.1) is modeled in the numerical analyses.

4.2 Results

Significant yielding occurred during crushing of the deck and hull plates and the internal structural members contained within the impact corner zone of the bow in all 24 analyses. All 24 numerical analyses were carried out until 36 in. of permanent deformation occurred at the elliptical corner region of the barge. As such, all (fully integrated) shell elements in the model of the bow were specified with a plastic-multilinear material model matching the stress-strain data derived from tests conducted on A-36 plate steel obtained for an actual barge. A large-displacement, large-strain formulation was used for the shell elements in the LS-DYNA impact analyses and the true (Cauchy) stress, true (logarithmic) strain data (Figure 2.7) specified for this material model for the A-36 steel. These test results were obtained from tests conducted at the University of Florida on a standard 18-inch tension coupon tested by Anderson and summarized in Consolazio et al. (2002).

4.3 Conclusions

This technical report provides a basis for revising the “capping force” cited in the April 2004 version of ETL 1110-2-563. The capping force is based on the computation of the “crushing” force imparted during a glancing blow of the impact corner at the bow of the impact barge with a lock approach wall. When placed in a severe impact environment in which the impact corner of the bow begins to “crush,” the impact corner at the bow acts like

a structural "fuse-plug" and provides for a limiting impact force applied to the approach wall by the barge train. The results of these 24 nonlinear finite element analyses of "crushing" of the barge impact corner definitively show a limiting force that may be transferred to a lock approach wall by the barge train through the front barge impact corner.

The magnitude of this limiting force ranges in value from 3,170 to 3,910 kips for the 24 analyses. The deformation corresponding to this first peak force is dependent upon the approach angle; it occurred at permanent normal deformations of about 5 in. for a 5° approach angle; about 6 in. for a 10° approach angle; about 11 in. for a 20° approach angle; and at about 15 in. for a 35° approach angle.

Table 4.1 summarizes the mean, standard deviation, and coefficient of variation (COV) values for the peak forces grouped by the approach angle using the Table 3.3 data. Table 4.1 results show that for each of the four approach angle data groups (i.e., 5°, 10°, 20°, and 35°), the average peak force values are within a narrow range of 3,420–3,590 kips. The COV (i.e., the dispersion about the first peak mean force value) is less than 5% for approach angles of 20° or less and is equal to 10% for an approach angle of 35°.

Table 4.1. Summary of mean, standard deviation, and coefficient of variation of the computed maximum force values for the 24 LS-DYNA runs.

Impact Angle	Case	First Peak Maximum Force		
Θ (°)	No.	Mean Force (kips)	Standard Deviation of Force (kips)	COV of Force (kips)
5	1—4	3,623	22.470	0.006
10	5—12	3,472	95.955	0.028
20	13—20	3,418	161.816	0.047
35	21—24	3,589	359.152	0.100

References

Arroyo, J. R., R. M. Ebeling, and B. B. Barker. 2003. *Analysis of impact loads from full-scale, low velocity, controlled barge impact experiments, December 1998*. ERDC/ITL TR-03-3. Vicksburg, MS: U.S. Army Engineer Research and Development Center.

Arroyo, J. R., and R. M. Ebeling. 2004. *A numerical model for computing barge impact forces based on ultimate strength of the lashings between barges*. ERDC/ITL TR-04-2. Vicksburg, MS: U.S. Army Engineer Research and Development Center.

_____. 2005. *Barge train maximum impact forces using limit states for the lashings between barges*. ERDC/ITL TR-05-1. Vicksburg, MS: U.S. Army Engineer Research and Development Center.

_____. 2006. Glancing-blow impact forces by a barge train on a lock-approach wall. *ASCE Journal of Infrastructure Systems* 12(2):135–143.

Bathe, K. J., J. Walczak, O. Guillermin, P. A. Bouzinov, and H. Chen. 1999. Advances in crush analysis. *Computers and Structures* 72:31–47.

Consolazio, G. R., R. A. Cook, and G. B. Lehr. 2002. *Barge impact testing of the St. George Island causeway bridge. Phase I: feasibility study*. Structures Research Report No. 783 to Florida Department of Transportation, UF Project No. 4504-783-12, Contract No. BC-354 RPWO #23. Gainesville, FL: Department of Civil & Coastal Engineering, College of Engineering, University of Florida.

Consolazio, G. R., and D. R. Cowan. 2003. Nonlinear analysis of barge crush behavior and its relationship to impact resistant bridge design. *Computers and Structures* 81:547–557.

Grigoriev, I. S., E. Z. Meilikhov, and A. A. Radzig. 1997. *Handbook of physical quantities*. Boca Raton, FL: CRC Press.

Encarta Encyclopedia. 2004. *Encarta*. Redmond, CA: Microsoft Corporation.

Headquarters, Department of the Army. 1993. (rescinded) *Barge impact analysis*. Engineer Technical Letter 1110-2-338. Washington, DC: U.S. Department of the Army.

_____. 2004. *Barge impact analysis for rigid walls*. Engineer Technical Letter 1110-2-563. Washington, DC: U.S. Department of the Army.

Livermore Software Technology Corporation. 2007. *LS-DYNA keyword user's manual, Version 971*. Vol 1. Livermore, CA: Livermore Software Technology Corp.

Patev, R. C., B. B. Barker, and L. V. Koestler. 2003. *Full-scale barge impact experiments, Robert C. Byrd Lock and Dam, Gallipolis Ferry, West Virginia*. ERDC/ITL TR-03-7. Vicksburg, MS: U.S. Army Engineer Research and Development Center.

Rainsberger, R. 2006. *TrueGRID user's manual: a guide and a reference, Version 2.3.0*. Vols 1 and 2. Livermore, CA: XYZ Scientific Applications, Inc.

Sullivan, J. F. 1988. *Technical physics*. New York: Wiley.

Appendix A: Background—Full-Scale, Low-Velocity Controlled-Impact Barge Experiments and the Development of the Empirical Correlation

A.1 Summary of the full-scale, low-velocity controlled-impact barge experiments

In December 1998, full-scale, low-velocity, controlled barge impact experiments were conducted by Patev et al. (2003) at the decommissioned Gallipolis Lock at Robert C. Byrd Lock and Dam, Gallipolis Ferry, WV. One of the many goals of these experiments was to measure the actual impact forces normal to the wall using a load-measuring device. The focus of these experiments was to obtain and measure the baseline response of an inland waterway barge, quantify a multi-degree-of-freedom system during the impact, and investigate the use of energy-absorbing fenders. The full-scale experiment used a 297-m-long (975-ft), 15-barge, commercial barge train in a 3-by-5 configuration, as shown in Figure A.1. Each barge was a jumbo open-hopper design 10.67 by 59.45 m (35 by 195 ft) with rake barges at the front of the tow. The barges were ballasted with anthracite coal to a draft of 2.74 m (9 ft). The total weight of the flotilla was 267,000 kN (30,012 short tons) with a total mass of 27,228,228 kg (1,865.59 kips-sec^2/ft), which is equal to the total weight divided by the gravitational constant, g. A total of 44 impact experiments were successfully conducted against the unaltered guide wall and a prototype fendering system that was attached to the wall. Approach velocity for the 12 bumper experiments conducted at the lock, ranged from 268 mm/sec to 875 mm/sec (0.88−2.87 ft/sec [fps]), with approach angles (θ) ranging from 8.8 to 21.1 . These shallow approach angles are typical of the approach angles with lock approach walls during glancing blow impacts. For each of these tests, the barge train was brought in at a constant approach angle θ and at a constant velocity. The target area was the stiff-to-rigid concrete upper guide wall, *lacking* the friction-reducing steel armor found on modern lock walls. The approach angle and velocity for the 12 most credible bumper experiments are summarized in Table A.1.

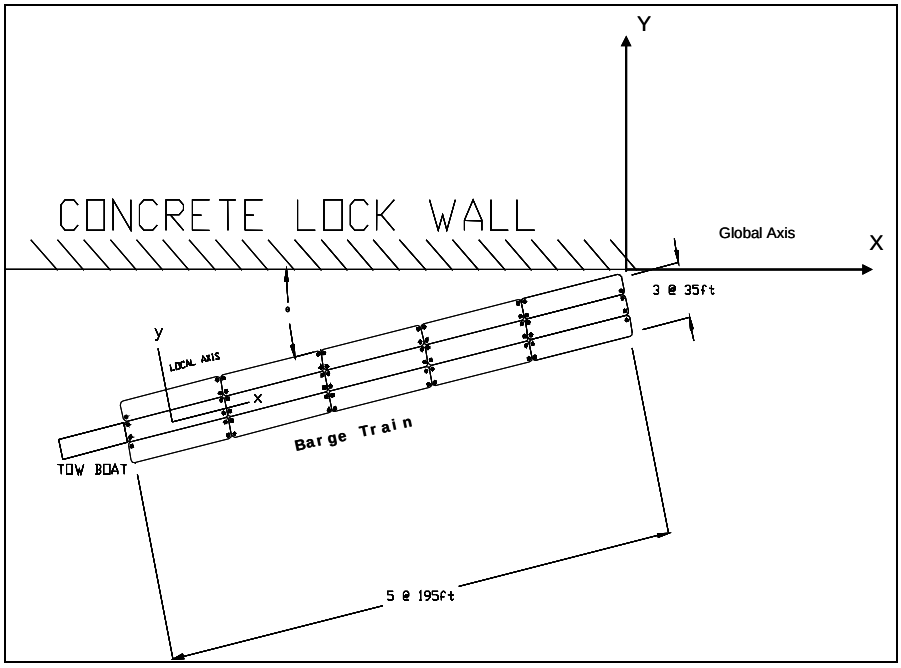

Figure A.1. Barge train-wall system.

Table A.1. Impact velocity/angle data for bumper experiment.

Experiment No.	Impact Angle, °	Velocity		Velocity Normal to the Wall	
		fps	mph	fps	mph
28	9.7	2.41	1.64	0.41	0.28
29	12.7	2.21	1.50	0.48	0.33
30	12.2	2.35	1.60	0.50	0.34
31	10.6	1.62	1.10	0.30	0.20
37	10.3	1.96	1.33	0.35	0.24
38	11.9	1.84	1.25	0.38	0.26
39	14.1	1.62	1.10	0.39	0.27
40	17.5	1.91	1.30	0.57	0.39
41	8.8	2.87	1.95	0.44	0.30
42	17.5	1.84	1.25	0.55	0.38
43	21.1	0.88	0.60	0.32	0.22
44	20.90	1.22	0.83	0.44	0.30

The load bumper (or, more specifically, the arc load beam) used to record the impact force time histories during the experiments was constructed of mild-steel with an outer radius of 72.6 in., outer arc length of 43.6 in., cross section measuring 9 in. in width by 5 in. in height, and separation between the 6-inch diameter load pins of 35.5 in.. The interpretation of the instrumentation data recorded by Patev et al. (2003) is discussed in Arroyo et al. (2003). The following summarizes key aspects of the Arroyo et al. interpretation. Once the time of impact was identified, the impact angle (the angle formed by the port side of the corner barge with the lock wall) was determined from the global positioning system (GPS) data corrected. This angle is critical to the bumper geometry and resulting force system. Velocity (actually speed) is simply calculated from the displacement of the front corner GPS unit per unit time (1 second). The initial orientation of the bumper relative to the longitudinal axis of the barges was adopted to be 54° from the longitudinal axis (local axis of the model) of the barges. Initially, the recorded forces at the pins were assumed to be in the radial direction. The precise orientation of the bumper on the barge is critical to this effort. The as-built orientation of the bumper was then determined from a combination of design drawings and documentary photos. The survey data were intended for this purpose; however, the uncertainty caused by the barges shifting and the tow drifting against its moorings between sightings compromised the accuracy of these measurements sufficiently to make them unusable for this purpose.

Subsequently, it was established from the design drawings and documentary photographs that the orientation of the recorded forces was not aligned in the radial direction of the arc load beam. Taking into account this observed discrepancy, a new orientation of the recorded forces was established. This second configuration was analyzed considering the magnitude of the angles associated with the orientation of the recorded forces. The results of this analysis indicated that an impossible geometrical arrangement was produced by this second set of assumptions. A final geometrical configuration was then established based on: (1) the range of probable angles for the force orientations relative to the radial direction, (2) the location of the bumper related to the longitudinal axis of the barges, and (3) the appropriate coefficient of friction between concrete (for the unarmored wall face) and (barge corner) steel. Arroyo et al. (2003) demonstrated that this final configuration produces reasonable results based on the values of the coefficient of friction between the wall and the steel bumper found in the technical literature, using the fact that the

bumper must be in compression during the impact process. Based on a careful assessment of the results from this bumper study, only eight of the initial 12 bumper impact experiments were used in the empirical correlation developed by Arroyo et al. (2003) to estimate the maximum impact force normal to the wall.

A.2 Background—empirical correlations

Using values for the maximum normal force F_w and the linear momentum normal to the wall, a best-fit straight line was calculated for the eight good experiments of 1998. This approach relates the maximum F_w obtained from the experiments directly to the linear momentum. The least-squares regression procedure was used to develop the best-fit straight line through the eight data points for the empirical correlation. The line was assumed to start at the origin (i.e., no intercept term was used for the linear equation). The resulting best-fit equation for this set of eight data values was $(F_w)_{max}$ = 0.435 mV sin θ. That is, a coefficient times the linear momentum normal to the wall determines the maximum force normal to the wall. We can observe that the greater the magnitude for the linear momentum, the larger the maximum value for the impact force normal to the wall. This relationship was based on low velocity, shallow impact (up to 21.1°) experiments that, by definition, do not account for factors that manifest themselves at higher velocities. Additionally, no damage occurred to the barge train and no lashings broke during these eight impact experiments.

The empirical correlation between the maximum force normal to the wall and the linear momentum normal to the wall immediately before impact developed using the Patev et al. (2003) field data; development of empirical correlation described in Arroyo and Ebeling (2004) and Arroyo et al. (2003) was based on statistical procedures and the values of force obtained from the acceptable bumper configuration.

The mathematical form of Newton's second law states that a resultant external force applied to a body is equal to the mass of the body multiplied by the absolute acceleration the body experiences. Furthermore, it can be expressed in terms of the absolute velocity of the body by introducing the first derivative with respect to time of the velocity, which is the acceleration. One useful tool that can be derived from Newton's second law, $F = ma$, is obtained by integrating both sides of the equation with respect to time. This integration can be done only if the forces acting on the particle are known functions of time. The external forces acting on the particle

change the linear momentum. The mathematical form of the resulting expression after the process of integration states that the impulse during a period of time due to the applied impulsive force is equal to the difference in linear momentum during the same interval of time. This relationship establishes the *Principle of Impulse and Linear Momentum*. The units of both impulse and momentum are force and time; therefore, impulse and momentum are expressed in Newton-sec, or kips-sec. The impulsive force is a function of time and, in general, varies during its period of application. A large force that acts over a short period of time is called an *impulsive force*.

The linear momentum is defined as the mass of the particle multiplied by the velocity of the particle. It is a vector quantity oriented in the same direction as the velocity of the particle (tangent to the trajectory). The velocity of a barge train is usually specified in the local barge axis: longitudinal, local "x" axis, and transverse, local "y" axis. In this case two velocities are specified, V_x and V_y. To obtain the velocity normal to the wall, an axis transformation equation is needed. This expression is the following:

$$\begin{Bmatrix} V_{par} \\ V_{norm} \end{Bmatrix} = [C]^{-1} \begin{Bmatrix} V_x \\ V_y \end{Bmatrix} \tag{A.1}$$

where $[C]^{-1} = \begin{bmatrix} \cos\theta & -\sin\theta \\ \sin\theta & \cos\theta \end{bmatrix}$, and V_{par} and V_{norm} are the velocity parallel (global "X" axis) and normal (global "Y" axis) to the wall, respectively. Equation A.1 can be obtained easily from Figure A.2.

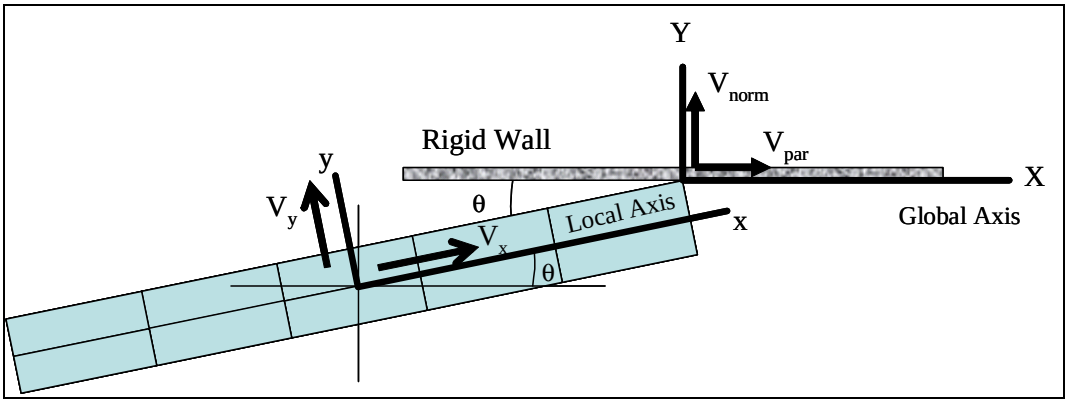

Figure A.2. Velocity vector transformation, from local to global axis (Arroyo and Ebeling 2006).

The empirical correlation between the maximum force normal to the wall and the linear momentum normal to the wall immediately before impact, developed by Arroyo et al. (2003) was based on statistical procedures and the values of maximum impact force obtained from the acceptable bumper configuration. Using values for the maximum normal force F_W and the linear momentum normal to the wall, a best-fit straight line was calculated using data from eight of the full-scale impact experiments. This approach relates the maximum F_W directly to the linear momentum. It is important to note that only one data point of the entire F_W time history for each of the eight experiments were used to develop this empirical correlation. The least-squares regression procedure was used to develop the best-fit straight line through the eight data points (for the eight impact experiments) for the empirical correlation. The line was assumed to start at the origin (i.e., no intercept term was used for the linear equation). The resulting best-fit straight line, average –1 standard error, and average +1 standard error lines were developed and shown in Figure A.3. The resulting best-fit equation for this set of eight data values is $(F_w)_{max}$ = 0.435 mV_{norm}, with units of the resulting force in kips, mass (including the mass of the loaded barges and tow boat, but excluding hydrodynamic added mass) in kips-sec^2/ft, and approach angle in degrees. That is, a coefficient times the linear momentum normal to the wall determines the maximum force normal to the wall. We can observe that the greater the magnitude for the linear momentum, the larger the maximum value for the impact force normal to the wall. This relationship was based on low-velocity, shallow impact (up to 21.1°) experiments that, by definition, do not account for factors that manifest themselves at higher velocities. Additionally, no damage occurred to the flotilla of barges and no lashings broke during these eight impact experiments. This empirical correlation was derived using data obtained from a barge train (3-by-5) that had a velocity normal to the wall up to and not exceeding 173.74 mm/sec (0.57 fps) with no damage occurring during impact events; this was up to 21.1° for impact angles, and 2,885.29 kN-sec (between 649.84 and 1,025.48 kips-sec) for a barge train with a linear momentum normal to the wall.

The maximum normal force $(F_W)_{max}$ by the empirical correlation is equal to the reaction force provided by the lock wall on the barge train during the impact. Note that the masses used to develop the correlation of linear momentum normal to the wall with values of $(F_W)_{max}$ uses the mass of the barge train and does not include the computation of any hydrodynamic added masses. (However, hydrodynamic effects on the barge train are

accounted for in the measured impact forces.) A single lumped mass was used to characterize the barge train in this simplified correlation.

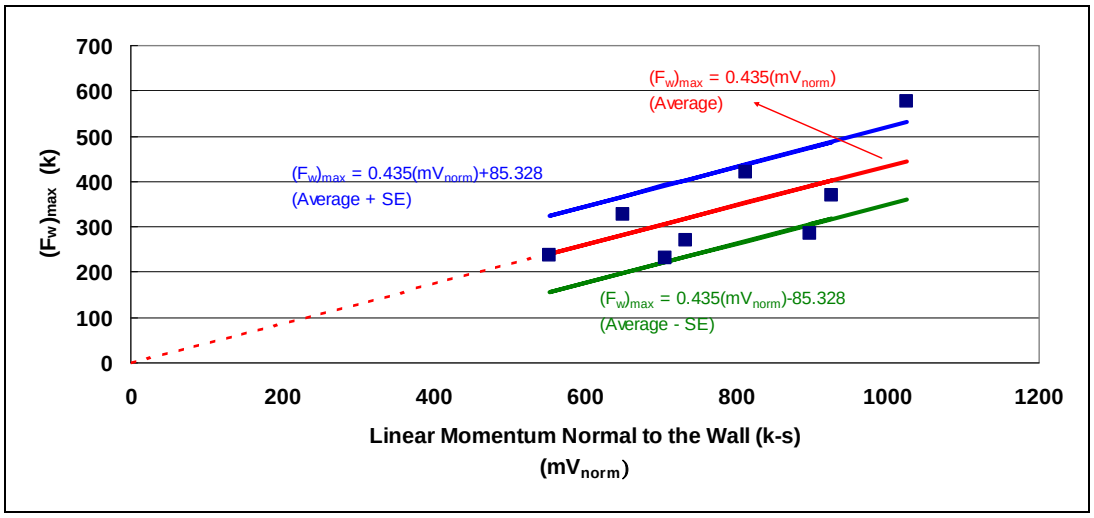

Figure A.3. Empirical correlation using the linear momentum normal to the wall concept (Figure 6.3 in Arroyo et al. 2003).

Appendix B: Effect of Number of Processors on LS-DYNA Runs

B.1 Cray XT-3

The 24 analyses that are the focus of this report were run on a Cray XT-3 supercomputer located in the High Performance Computing (HPC) center of USACE, Engineer Research and Development Center. The XT-3 is a Massively Parallel Processor supercomputer that contains 4,160 nodes, each containing one 2.6-GHz AMD Opteron 64-bit dual-core processor and dedicated memory. Compute nodes comprise 4,096 of the nodes, which, together, have 4 GB of RAM. The remaining 64 nodes are service nodes. The operating system is UNICOS/lc.[1]

B.2 LS-DYNA multiprocessor capability

LS-DYNA is capable of using this parallel architecture. When running LS-DYNA, the user may specify the number of processors to use in completing the task. LS-DYNA decomposes the model into a number of pieces to fit the number of processors specified.

B.3 Glancing blow analyses run times

Analyses are performed by submitting each run as a job to a batch queue. Jobs run as resources become available. There are practical considerations involved in deciding the number of processors to specify in running a job. A small number of processors requires a longer actual elapsed time for a job to run than a large number of processors. However, the time a job spends waiting in the job queue increases as the number of processors requested increases. For that reason, the number of processors used to run the jobs for these analyses varied.

The 24 analyses performed as part of this study involved normal velocities that spanned a range of 0.6425–50.1443 in./sec. To obtain a displacement of 36 in., the LS-DYNA model times varied from 57.6 seconds down to 0.75 seconds. A model time of 0.75 seconds completed in an actual elapsed time of 31.675 hours, using four processors to run. Attempting to run a

[1] This information was obtained from the HPC Website http://www.erdc.hpc.mil/systemNews/Cray_XT3/ug#configuration.

model time of 57.6 seconds on four processors would have required over 101 days. Obviously, that is not practical. To obtain results in a timely fashion, the authors decided to perform analyses using the number of processors shown in Table B.1.

Table B.1. Number of processors used for glancing blow runs.

Case No.	Number of Processors
1	512
2	256
3	256
4	256
5	256
6	256
7	256
8	256
9	256
10	256
11	256
12	256
13	4
14	4
15	4
16	4
17	4
18	4
19	4
20	4
21	4
22	4
23	4
24	4

B.4 Sensitivity of computed results to the number of processors specified

To satisfy themselves that LS-DYNA results were not dependent on the decomposition of a problem, the authors performed analyses of Case No. 18 using 4, 32, 64, and 256 processors. The computed force normal to the approach wall versus-displacement normal to the wall results obtained from the four analyses are shown in Figure B.1 for the fully integrated shell element (*SECTION_SHELL; ELFORM 16) with a plastic-multilinear material model (LS-DYNA material No. 24, *MAT_PIECEWISE_LINEAR_PLASTICITY).

Figure B.1 shows that consistency in results between the four runs is excellent out to approximately 17 in. of permanent deformation. Past that displacement there is not total agreement in the computed results, but it was concluded by the authors of this report that the results are consistent, except for some acceptable, minor differences. It cannot be understated that there is significant plastic response and erosion of elements at this stage of the nonlinear analysis; the computations may be sensitive to small changes in plastic responses and element erosion during the course of nonlinear analyses of the multi-degree-of-freedom structural barge bow system. The end result in a nonlinear analysis depends upon the path taken. Considering these issues, the authors are content that for the fully integrated shell element, the computed results are not sensitive to the number of processors specified in the analysis.

To save execution time, a similar parametric study on the accuracy in results to the number of processors for the LS-DYNA reduced integrated shell elements (*SECTION_SHELL; ELFORM = 2; NUMBER OF INTEGRATION POINTS = 3) with hourglass control (*HOURGLASS; Hourglass Control Type = 4, Flanagan-Belytschko stiffness form) was performed. However, in plots of the force versus permanent displacement normal to the wall (similar to Figure B.1), it is observed that the computed results varied significantly in the nonlinear, plastic portion of the contact force response if the number of processors used to run a problem varied. Therefore, only the fully integrated shell element model was specified for the computations reported in this technical report.

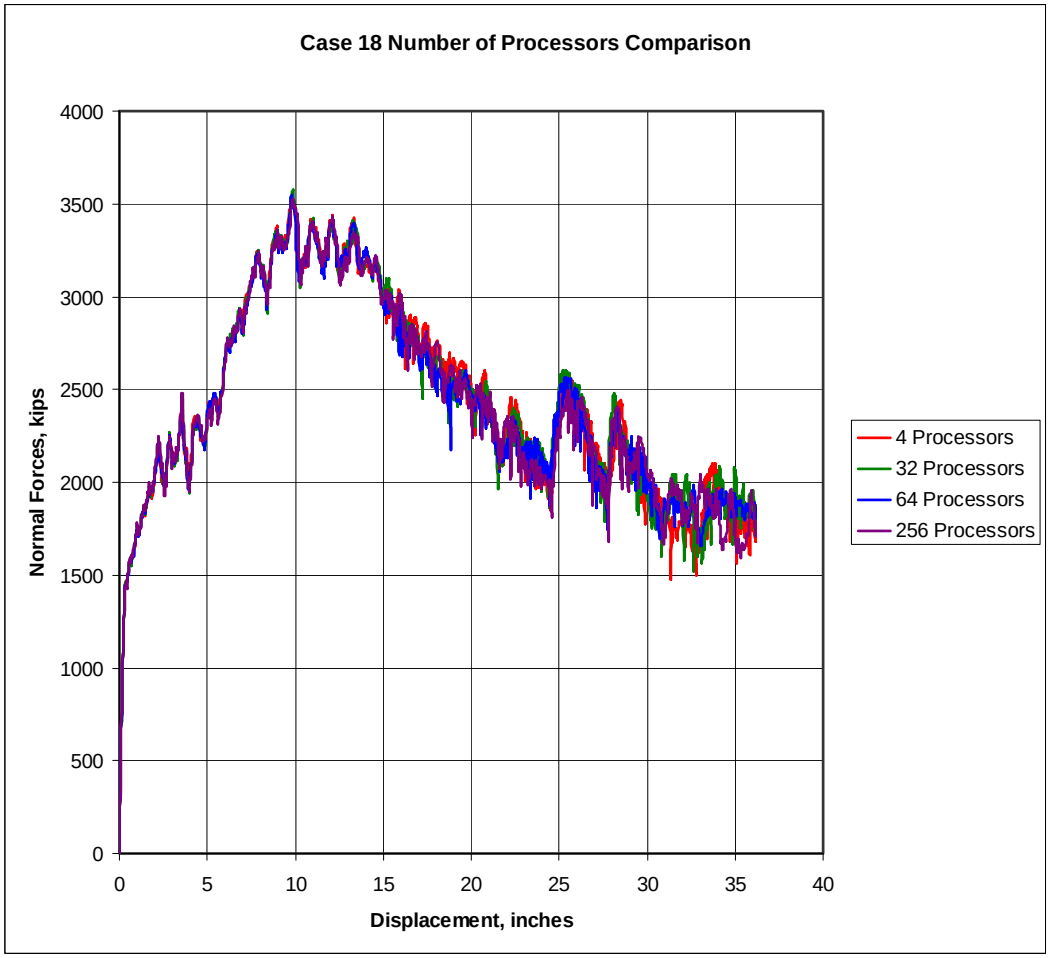

Figure B.1. Results obtained with four different problem decompositions for Case No. 18.

REPORT DOCUMENTATION PAGE

Form Approved
OMB No. 0704-0188

1. REPORT DATE *(DD-MM-YYYY)*	**2. REPORT TYPE**	**3. DATES COVERED** *(From - To)*
November 2008	Final report	

4. TITLE AND SUBTITLE

Limiting Impact Force Due to Yielding and Buckling of the Plates and Internal Structural Frame at the Impact Corner of the Barge during Its Glancing Blow Impact with a Lock Approach Wall

5a. CONTRACT NUMBER

5b. GRANT NUMBER

5c. PROGRAM ELEMENT NUMBER

6. AUTHOR(S)

Robert M. Ebeling and Terry W. Warren

5d. PROJECT NUMBER

5e. TASK NUMBER

5f. WORK UNIT NUMBER
0HB385

7. PERFORMING ORGANIZATION NAME(S) AND ADDRESS(ES)

U.S. Army Engineer Research and Development Center
Information Technology Laboratory
3909 Halls Ferry Road
Vicksburg, MS 39180-6199

8. PERFORMING ORGANIZATION REPORT NUMBER
ERDC/ITL TR-08-2

9. SPONSORING / MONITORING AGENCY NAME(S) AND ADDRESS(ES)

Headquarters, U.S. Army Corps of Engineers
Washington, DC 20314-1000

10. SPONSOR/MONITOR'S ACRONYM(S)

11. SPONSOR/MONITOR'S REPORT NUMBER(S)

12. DISTRIBUTION / AVAILABILITY STATEMENT

Approved for public release; distribution is unlimited.

13. SUPPLEMENTARY NOTES

14. ABSTRACT

In 2003, the U.S. Army Corps of Engineers issued ERDC/ITL TR-03-3, which interpreted eight of the 44 full-scale, low-velocity, controlled-impact barge train experiments conducted at the decommissioned Gallipolis Lock at Robert C. Byrd Lock and Dam. An easy-to-use "empirical correlation" was derived, reporting the maximum impact force (normal to the wall) as a function of the linear momentum normal to the wall (immediately before impact). This empirical correlation was cited in ETL 1110-2-563 (April 2004) for impacts with stiff-to-rigid walls that do not involve damage to either the corner barge or the wall; a limiting impact force of 800 kips (capping the empirical correlation) was cited. In this technical report, we provide a basis for revising the "capping force" cited in ETL 1110-2-563, based on the computation of the "crushing" force imparted during a glancing blow of the impact corner at the bow with a lock approach wall.

A second limiting force due to the limit state of lashing forces during a glancing blow impact is addressed in the USACE technical report ERDC/ITL TR-05-1. The lower of the two limiting forces—due to the crushing of the barge impact corner or to the failure of the lashings—"caps" the empirical correlation.

15. SUBJECT TERMS

Barge; Crush analysis; Glancing blow; Impact; Limiting impact force for a barge train; Lock approach wall; LS-DYNA; Nonlinear finite element analysis; Plate buckling

16. SECURITY CLASSIFICATION OF:			**17. LIMITATION OF ABSTRACT**	**18. NUMBER OF PAGES**	**19a. NAME OF RESPONSIBLE PERSON**
a. REPORT	**b. ABSTRACT**	**c. THIS PAGE**			**19b. TELEPHONE NUMBER** *(include area code)*
UNCLASSIFIED	UNCLASSIFIED	UNCLASSIFIED		56	